

A Bayesian approach for the modelling of material stocks and flows with incomplete data

Junyang Wang¹ Kolyan Ray³ Pablo Brito-Parada² Yves Plancherel²
 Tom Bide⁵ Joseph Mankelaw⁵ John Morley² Julia Stegemann⁴
 Rupert Myers¹

November 14, 2022

Abstract

Abstract. Material Flow Analysis (MFA) is used to quantify and understand the life cycles of materials from production to end of use, which enables environmental, social and economic impacts and interventions. MFA is challenging as available data is often limited and uncertain, giving rise to an underdetermined system with an infinite number of solutions when attempting to calculate the values of all stocks and flows in the system. Bayesian statistics is an effective way to address these challenges as it rigorously quantifies uncertainty in the data and propagates it in a system flow model to provide the probabilities associated with model solutions. Furthermore, the Bayesian approach provides a natural way to incorporate useful domain knowledge about the system through the elicitation of the prior distribution.

This paper presents a novel Bayesian approach to MFA. We propose a mass based framework that directly models the flow and change in stock variables in the system, including systems with simultaneous presence of stocks and disaggregation of processes. The proposed approach is demonstrated on a global aluminium cycle, under a scenario where there is a shortage of data, coupled with weakly informative priors that only require basic information on flows and change in stocks. Bayesian model checking helps to identify inconsistencies in the data, and the posterior distribution is used to identify the variables in the system with the most uncertainty, which can aid data collection. We numerically investigate the properties of our method in simulations, and show that in limited data settings, the elicitation of an informative prior can greatly improve the performance of Bayesian methods, including for both estimation accuracy and uncertainty quantification.

Keywords. Material flow analysis • Bayesian statistics • Probabilistic modelling • Uncertainty quantification • Missing data • Circular Economy

1 Introduction

Increasingly, the world is facing major shifts in resource utilisation. To prevent the worst consequences of climate change, global carbon emissions must be significantly reduced, which requires a fundamental change in how fossil fuels and other high carbon footprint materials are used in the coming decades. Additionally, the current instability of supply chains, changing behaviour caused by Covid-19 (Jowitt [2020]), as well as the growing world population, projected to reach almost 10 billion by 2050 (WPP [2022]), will also likely significantly impact resource utilisation globally (Jowitt et al. [2020]). However, currently many material flows of interest are poorly understood, which severely impedes the ability of policy makers to identify ways to use important materials or resources more efficiently and sustainably,

¹ Department of Civil and Environmental Engineering, Imperial College London, United Kingdom. junyang.wang21@imperial.ac.uk, r.myers@imperial.ac.uk

² Department of Earth Science and Engineering, Imperial College London, United Kingdom. p.brito-parada@imperial.ac.uk, y.plancherel@imperial.ac.uk, john.morley18@imperial.ac.uk

³ Department of Mathematics, Imperial College London, London, United Kingdom. kolyan.ray@imperial.ac.uk

⁴ Department of Civil, Environmental and Geomatic Engineering, University College London, London, United Kingdom. j.stegemann@ucl.ac.uk

⁵ British Geological Survey, United Kingdom. tode@bgs.ac.uk, jmank@bgs.ac.uk

and plan the transition to more sustainable systems of production and use (Mudd [2021], UNE [2020]). Additionally, this complexity makes it more difficult for industry to reduce environmental impacts and increase profits systemically across their activities and product life cycles. Therefore, it is important that the entire life cycle of materials of interest is mapped and quantified reliably, from extraction to production to use to disposal and recycle and reuse.

Material flow analysis (MFA) is a broad terminology encompassing any quantitative method used to map and quantify flows and stocks of a material of interest in a well defined system. MFA is applicable to all materials and a range of economic, environmental and social scales, from a company's supply chain to entire countries and economies. MFA studies have been conducted on metals, including steel and aluminium (Bertram et al. [2009] and Cullen et al. [2012]), non-metals such as glass and concrete (Westbroek et al. [2021] and da Costa Reis et al. [2019]), for entire countries (Matsubae-Yokoyama et al. [2009]), on a global scale (Miatto et al. [2017]) and for multiple materials across whole economies (Fischer-Kowalski et al. [2011]). Common to all MFA models is the precise definition of a system, which includes the system boundary, the processes within this system, as well as stock and flow variables representing the storage within and movement between the processes. A physical assumption common to all MFA models is the conservation of mass, where the outflows and inflows of a process must balance with its change of stock.

Typically in MFA problems it is difficult or impossible to collect data for all the stock and flow variables inside the system, because in real systems there are many such variables. Therefore, the size of the set of available data combined with physical constraints, containing at least mass balance of processes, is usually still less than the number of variables, even after simplification of the real system modelled. For modelling this gives rise to an underdetermined system which places MFA datasets in the domain of high dimensional statistics (Lederer [2022]). Well known statistical methods in this area include ridge regression, the LASSO, Elastic net, as well as Bayesian approaches (Hoerl and Kennard [2000], Tibshirani [1996], Zou, Kruschke [2015]).

This paper focuses on developing a new Bayesian MFA method. Bayesian statistics is particularly well suited for MFA for three main reasons. Firstly, Bayesian statistics works naturally in the underdetermined setting by providing a posterior probability over all possible solutions instead of a single solution. Secondly, while commonly there is a lack of data in MFA problems, there is often domain knowledge or expert opinion that can be used to greatly improve the prediction accuracy of the model, and the Bayesian prior distribution provides a natural framework to incorporate such domain knowledge, which is missed in the traditional MFA approach. Thirdly, Bayesian statistics rigorously quantifies uncertainty in the data and propagates it into the posterior distribution. The posterior can continue to update itself with more data as they become available, increasing the accuracy and decreasing the uncertainty on the unknown variables in an iterative fashion.

The use of Bayesian statistics in MFA is still relatively limited. Perhaps the earliest use of Bayesian statistics in MFA is by Gottschalk et al. [2010], in which the authors modelled stock variables representing concentrations of nanoparticles in the environment via conservation of mass. In Lupton and Allwood [2018], the authors argued for an incremental approach to MFA, perhaps first proposed by Brunner and Rechberger [2004], where a Bayesian model is constructed during the data collection process to provide uncertainty quantification. Lupton and Allwood [2018] proposed a Bayesian model framework in which prior distributions are elicited over flow ratios known as transfer coefficients of a material flow system, and conducted a case study mapping global steel flows. Recently, Dong et al. [2022] proposed a method which combines prior information from multiple experts in the MFA setting, demonstrating it on the model of Lupton and Allwood [2018].

Bayesian methods have also been adopted in the related area of data reconciliation in mass balanced systems. Unlike MFA, the main goal of data reconciliation is to reconcile repeated measurements of the same variable, rather than filling in missing data gaps. Data reconciliation typically deals with datasets where the data or sample size (including constraints like conservation of mass) is greater than the number of variables of interest. Past works in this area include Cencic and Frühwirth [2015, 2018], Koermer and Noble [2021].

This paper presents a novel Bayesian methodology for material flow analysis. We employ a different model parametrisation compared to existing Bayesian MFA methods based on transfer coefficients, in which priors are elicited directly over the stock and flow mass variables in the material system, while retaining the ability to incorporate flow ratio data. Furthermore, unlike previous approaches, we

demonstrate our Bayesian approach on more sophisticated material flow systems where stocks and disaggregation of processes and flows are simultaneously present, which is a common feature in material flow datasets (Myers et al. [2019a] and Myers et al. [2019b]). We demonstrate our model provides full posterior inference including point estimation as well as uncertainty quantification, for all stock and flow variables inside the system, including at the lowest level of disaggregation where data is often unavailable. We illustrate how Bayesian methods of model checking can reveal inconsistencies in the data, and the posterior can aid data collection strategies by identifying which stocks or flows in the system retain the most uncertainty. Lastly, we conduct simulation studies to examine the estimation accuracy and uncertainty quantification of the posterior distributions of our model.

2 Methods

In this section, we present the details of our proposed Bayesian MFA methodology. We developed a Bayesian parametric model that produces estimates and uncertainty quantification of all flow and change in stock variables of interest in any given material flow system, in the form of a posterior distribution, which combines prior domain knowledge and expert opinion with available data while simultaneously quantifying and propagating uncertainty.

A MFA analysis begins with the definition of a *system diagram*, a graph like structure of nodes representing *processes*, where the material of interest can be stored as stock, and edges representing *flows* of the material of interest between processes. Notably however, flows in both directions between any two processes are permitted. The system diagram will also contain a system boundary, which is used to describe the flows between the system and some external environment. This framework is quite broad, and allows processes within a system to not only represent a physical manufacturing process (such as components of a blast furnace), but also examples such as the Earth’s lithosphere, the environment, or various usage outlets like households where the material of interest can be stored or flow in and out of. Similarly, the system’s scope can range from a small supply chain of a company, to an country’s material flow of a metal such as zinc. The level of detail of the system diagram is chosen by the modeller to fit the scope of the problem being examined.

Often in MFA problems, certain processes in the system can be disaggregated into constituent subprocesses (see e.g. Myers et al. [2019b]). We define a *parent process* to be a process which contains subprocesses, and a *child process* be a process which contains no subprocesses instead. By definition, parent and child processes form a partition of the set of all processes in the system. It may be possible to disaggregate child processes further from a physical point of view, but from a modelling perspective there is no interest to do this and thus the more disaggregated processes are excluded from the system scope.

The parent and child process structure is useful for modelling the disaggregation of processes. To see this, we assume the stocks and flows of any parent process can be expressed as a linear combination of its constituent child processes. Under this parent and child process framework, multiple levels of disaggregation of processes can be reduced to just two levels (the set of parent processes and the set of child processes), which greatly simplifies modelling of the MFA system. Furthermore, Bayesian modelling only needs to be conducted on the child processes, as the posterior samples on stocks or flows of parent processes can be obtained by simply summing the posterior samples of the constituent child processes. A simple example illustrating the parent and child process framework can be found in the supplementary information.

2.1 Formulation of the physical model

Suppose there are m child processes in the system, indexed by P_0, P_1, \dots, P_{m-1} . We let $s_i(t)$ to be the stock variable associated with the process P_i , denoting the amount of stock in process P_i at time t . We let the flow rate variables $u_{j,k}(t)$ denote the rate of flow from process P_j into process P_k at time t . Note typically in MFA systems not all processes necessarily possess a stock variable, for example if the physical process which it is modelling does not contain a physical stock of the material of interest. Similarly, most processes will not receive flows from or flow to every other process, so the notation introduced in this paragraph such as s_i and $u_{j,k}$ are understood to be over existing stocks and flow variables only. For each process P_i , we assume mass is conserved between its stock, inflows and outflows, which we formulate as:

$$\frac{ds_i(t)}{dt} = \sum_j u_{j,i}(t) - \sum_k u_{i,k}(t) \quad (1)$$

In practice material flow data are typically recorded as the total amount of flow over a period time (such as on a monthly or yearly basis), so equation (1) cannot be immediately be related to the data recorded. To make use of the conservation of mass equations, we integrate the equation (1) over the period for which the data was recorded, which we denote by the period between $t - \Delta t$ and t (Δt here represents the period during which the total amount of flow was reported, which can for example be in months or years), in order to obtain:

$$\int_{t-\Delta t}^t \frac{ds_i(t)}{dt} dt = \int_{t-\Delta t}^t \left(\sum_j u_{j,i}(t) - \sum_k u_{i,k}(t) \right) dt$$

$$S_i = s_i(t) - s_i(t - \Delta t) = \sum_j U_{j,i} - \sum_k U_{i,k} \quad (2)$$

where $U_{j,i} = \int_{t-\Delta t}^t u_{j,i}(t) dt$ represents the total amount of flow of the material of interest from process j to process i during the time period $t - \Delta t$ to t , which is typically the form of flow data that is recorded in practice. The left hand side $S_i = s_i(t) - s_i(t - \Delta t)$ is simply the change in stock during the time period t to $t - \Delta t$. In this paper we only consider stationary models at a snapshot of time t , so the variables of interest in the model are the S_i and $U_{j,k}$. For more compact notation, let \mathbf{S} be the vector of q change in stock variables S_i of the child processes in the system, and \mathbf{U} a vector of $p - q$ flow variables $U_{j,k}$ of the child processes in the system (for a total of p variables). Note because stocks and flows of parent processes can be expressed linearly in terms of its constituent child processes, conservation of mass for all child processes automatically implies conservation of mass for all parent processes.

2.2 Data structure

Data in MFA can in principle be any arbitrary function $f(\mathbf{S}, \mathbf{U})$ of the variables of interest \mathbf{S} and \mathbf{U} . However, data and mass balance conditions typically come in the following four forms, which we can express in terms of \mathbf{S} and \mathbf{U} :

1. Observations of changes in stock of child processes or observations of flows between child processes. For example, in [Figure 2](#), $S_0 = -37.2$ Mt/yr could be used to describe the change in stock of the ‘Reserves’ process, while the flow from ‘Reserves’ to ‘Mining’ can be described by $U_{0,1} = 37.2$ Mt/yr. Here the process ‘Reserves’ is labelled by P_0 and the process ‘Mining’ by P_1 . The indices assigned to processes here are arbitrary, but is consistent with the data provided in the supplementary material.

2. Observations of changes in stock of parent processes, or observations of flows between processes where at least one process is a parent, which can be treated as the sum of multiple flows. For example, the combined flow of 9.8 Mt/yr in [Figure 2](#) from ‘WasteManagement’ to ‘Recycling’ consists of ‘WasteManagement’ as the origin process, and the destination processes are ‘Remelting’ and ‘Refining’, two of the subprocesses of ‘Recycling’. This flow can be represented by the sum of flows $U_{31,7} + U_{31,8} = 9.8$ Mt/yr. Here we used P_{31} to denote ‘WasteManagement’, and P_7, P_8 ‘Remelting’ and ‘Refining’ subprocesses of ‘Recycling’ respectively. So for example, $U_{31,7}$ represents the flow from ‘WasteManagement’ to ‘Remelting’.

3. Conservation of mass. For child process i this is represented by

$$S_i - \sum_j U_{j,i} + \sum_k U_{i,k} = 0 \quad (3)$$

4. Ratio data between flows, for instance transfer coefficients:

$$\frac{U_{i,j}}{\sum_k U_{i,k}} = \alpha_{i,j} \quad (4)$$

where $\alpha_{i,j}$ is a known transfer coefficient of the flow from process i to process j , and is defined as the ratio between the flow from process i to process j , divided by the total outflow of process i . Ratio data can also be alternatively parametrised linearly in the following way:

$$U_{i,j} - \alpha_{i,j} \sum_k U_{i,k} = 0 \quad (5)$$

We note it is possible to conveniently formulate all the most common forms of data and mass balance conditions in MFA in terms of linear relationships between the change in stock variables S_i and the flow variables $U_{j,k}$, even when the system contains disaggregation of processes. However, for a more general framework and to demonstrate our model can incorporate nonlinear data as well, we choose to parametrise ratio data as Equation (4) when evaluating the model on the aluminium case study in the Results section.

Using more compact notation, the relationship between the stock and flow variables and the data and physical constraints can be represented by the following model:

$$\mathbf{Y} = \begin{bmatrix} X\boldsymbol{\theta} \\ \mathbf{R}(\boldsymbol{\theta}) \end{bmatrix} + \boldsymbol{\epsilon} \quad (6)$$

$$\boldsymbol{\theta} = \begin{bmatrix} \mathbf{S} \\ \mathbf{U} \end{bmatrix} \quad (7)$$

where $\boldsymbol{\theta}$ is a concatenated vector of \mathbf{S} and \mathbf{U} of length p . \mathbf{Y} is a vector of length n of observed values, or 0 for mass balance conditions. X is a design matrix representing linear data and mass balance conditions, and $\mathbf{R}(\boldsymbol{\theta})$ a vector representing nonlinear data. $\boldsymbol{\epsilon}$ is a random vector (of length n) representing uncertainty in the data, which could be caused by measurement or rounding errors. Note in the MFA setting, it is often the case that $n \ll p$.

The goal of any Bayesian model is to obtain posterior distributions over the variables of interest, in this case $\boldsymbol{\theta}$, in order to perform inference such as point estimation or uncertainty quantification. In the following section we describe how to construct the prior for our model, the form of the likelihood and how to obtain the posterior of $\boldsymbol{\theta}$ via Bayes's theorem.

2.3 Bayesian model detail

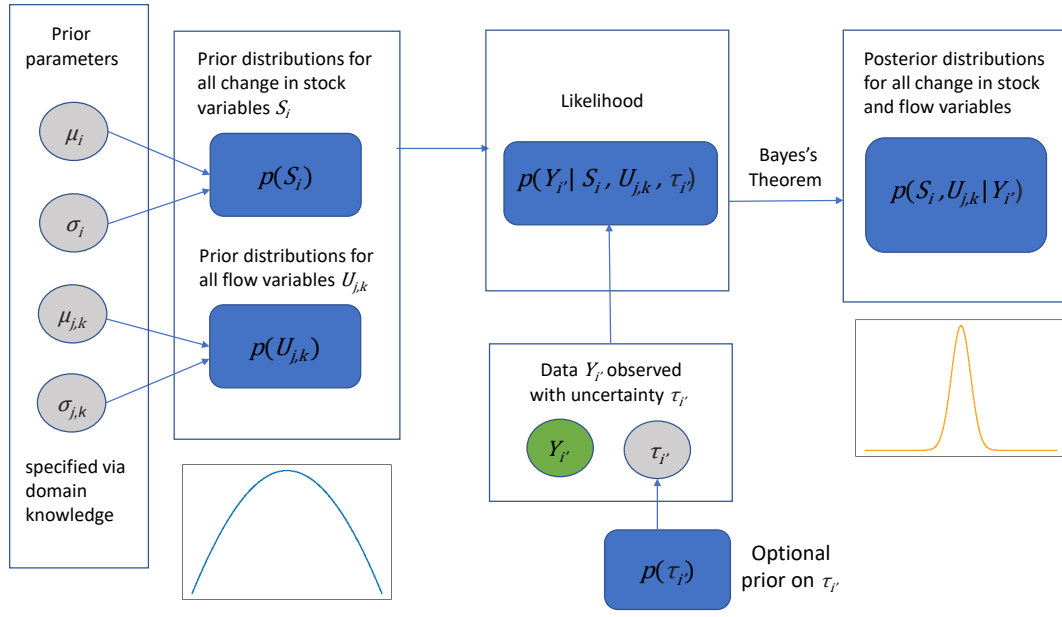
For our Bayesian model, we consider normal priors for the change in stock variables S_i , which reflects the fact that the change in stock can be both positive or negative. For the flow variables $U_{j,k}$, we consider truncated normal priors for the flow variables on the positive interval $[0, L]$, where L is chosen based on domain knowledge of the scale of flows inside the system being modelled. This is to ensure the posterior distribution of the flow variables have positive support, as flow quantities are always positive in reality. Furthermore, the normal and truncated normal distributions are flexible, in the sense that an informative prior distribution can be elicited by choosing the prior mode as a confident estimate (from expert knowledge), and choosing a small prior variance to create a narrow distribution around the prior mode. On the other hand, an uninformative prior distribution can be elicited by choosing a large prior variance around a rough guess for the prior mode instead.

$$S_i \sim \mathcal{N}(\mu_i, \sigma_i^2) \quad (8)$$

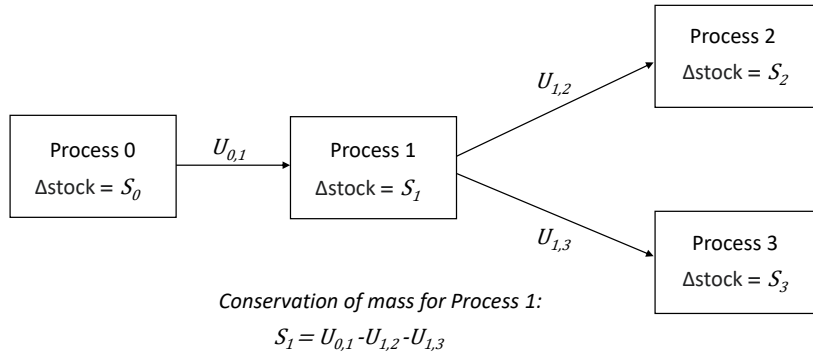
$$U_{j,k} \sim \mathcal{TN}(\mu_{j,k}, \sigma_{j,k}^2, 0, L) \quad (9)$$

where μ_i and σ_i^2 are the prior mean and variance of i th change in stock variable S_i , respectively, and $\mu_{j,k}$ and $\sigma_{j,k}^2$ the corresponding prior parameters respectively for the truncated normal distribution for the flow variable $U_{j,k}$, representing the flow quantity from process j to process k . We also assume prior variables are independent, so the overall prior distribution $p(\boldsymbol{\theta})$ over the change in stock and flow variables is of the form:

$$p(\boldsymbol{\theta}) \propto \prod_i \frac{1}{\sigma_i} \exp\left(-\frac{(S_i - \mu_i)^2}{2\sigma_i^2}\right) \prod_{(j,k)} \frac{1}{\sigma_{j,k}} \exp\left(-\frac{(U_{j,k} - \mu_{j,k})^2}{2\sigma_{j,k}^2}\right) \mathbb{I}_{U_{j,k} \in [0, L]} \quad (10)$$



(a)



(b)

Figure 1: Schematic of the Bayesian model (a), example of simple MFA system (b). The shapes coloured in grey represent model parameters, the shapes coloured in green represent the data and the shapes coloured in blue represent distributions over the variables of interest as well as the model likelihood. Definitions for each variable and parameter in this figure can be found in the Methods section.

where $\mathbb{I}_{U_{j,k} \in [0,L]}$ is an indicator function, and the products are over the stock variables S_i and flow variables $U_{j,k}$.

For the likelihood, we again use a truncated normal likelihood for any data on observed flow values to ensure the data generated by the likelihood is plausible (since flow data should be strictly positive), and a normal likelihood for data on observed change in stock values, mass conservation conditions and general nonlinear data.

$$Y_{i'}|\boldsymbol{\theta} \sim \mathcal{N}(\mathbf{x}_{i'}^\top \boldsymbol{\theta}, \tau_{i'}^2) \quad \text{for observations } Y_{i'} \text{ on change in stock data} \quad (11)$$

$$Y_{j'}|\boldsymbol{\theta} \sim \mathcal{TN}(\mathbf{x}_{j'}^\top \boldsymbol{\theta}, \tau_{j'}^2, 0, L') \quad \text{for observations } Y_{j'} \text{ on flow data} \quad (12)$$

$$Y_{k'}|\boldsymbol{\theta} \sim \mathcal{N}(R(\boldsymbol{\theta})_{k'}, \tau_{k'}^2) \quad \text{for observations } Y_{k'} \text{ on nonlinear data} \quad (13)$$

$$Y_{l'}|\boldsymbol{\theta} \sim \mathcal{N}(\mathbf{x}_{l'}^\top \boldsymbol{\theta}, \tau_{l'}^2) \quad \text{for } Y_{l'} = 0 \text{ on mass balance conditions} \quad (14)$$

$$(15)$$

Here $Y_{i'}$ is the i' th row or entry of the observation vector \mathbf{Y} , and $\mathbf{x}_{i'}^\top$ the i' th row of the design matrix X , $R(\boldsymbol{\theta})_{k'}$ the k' th row of the vector $\mathbf{R}(\boldsymbol{\theta})$ and $\tau_{i'}^2$ representing variance of the noise of the i' th observation, which are assumed to be independent. The overall likelihood $p(\mathbf{Y}|\boldsymbol{\theta})$ is therefore of the form:

$$p(\mathbf{Y}|\boldsymbol{\theta}) = \prod_{i'} p(Y_{i'}|\boldsymbol{\theta}) \prod_{j'} p(Y_{j'}|\boldsymbol{\theta}) \prod_{k'} p(Y_{k'}|\boldsymbol{\theta}) \prod_{l'} p(Y_{l'}|\boldsymbol{\theta}) \quad (16)$$

where

$$p(Y_{i'}|\boldsymbol{\theta}) \propto \frac{1}{\tau_{i'}} \exp\left(-\frac{(Y_{i'} - \mathbf{x}_{i'}^\top \boldsymbol{\theta})^2}{2\tau_{i'}^2}\right) \quad (17)$$

$$p(Y_{j'}|\boldsymbol{\theta}) \propto \frac{1}{\tau_{j'}} \exp\left(-\frac{(Y_{j'} - \mathbf{x}_{j'}^\top \boldsymbol{\theta})^2}{2\tau_{j'}^2}\right) \mathbb{I}_{Y_{j'} \in [0, L']} \quad (18)$$

$$p(Y_{k'}|\boldsymbol{\theta}) \propto \frac{1}{\tau_{k'}} \exp\left(-\frac{(Y_{k'} - R(\boldsymbol{\theta})_{k'})^2}{2\tau_{k'}^2}\right) \quad (19)$$

$$p(Y_{l'}|\boldsymbol{\theta}) \propto \frac{1}{\tau_{l'}} \exp\left(-\frac{(Y_{l'} - \mathbf{x}_{l'}^\top \boldsymbol{\theta})^2}{2\tau_{l'}^2}\right) \quad (20)$$

Given the prior and likelihood, we can then use Bayes's Theorem to obtain the posterior distribution $p(\boldsymbol{\theta}|\mathbf{Y}) = \frac{p(\boldsymbol{\theta})p(\mathbf{Y}|\boldsymbol{\theta})}{\int p(\boldsymbol{\theta})p(\mathbf{Y}|\boldsymbol{\theta})d\boldsymbol{\theta}}$. However, the posterior induced by this model does not admit an analytical form, and so we employ Markov Chain Monte Carlo (MCMC) methods to generate samples from the posterior. Specifically, we employ the Hamiltonian Monte Carlo No-U-Turn Sampler (NUTS) algorithm of Hoffman and Gelman [2014], implemented via the PyMC3 library Salvatier et al. [2016] in Python.

Optionally, for full Bayesian inference the model user can assign prior distributions to the variance parameter of the noise variables $\boldsymbol{\tau}$ over just using an plug in an estimate based on domain knowledge (such as 10% of the data value as in Lupton and Allwood [2018]). To this end we consider Inverse Gamma priors that are identically distributed and also independent of the prior on the change in stock and flow variables $p(\boldsymbol{\theta})$, which is of the form:

$$p(\boldsymbol{\tau}) \propto \prod_{i'} \exp\left(\frac{-b_{i'}}{\tau_{i'}}\right) \tau_{i'}^{-a_{i'}-1} \quad (21)$$

For the aluminium dataset used in this paper, we found that assigning the prior in Equation (21) significantly increases computational time of the NUTS algorithm and the resulting posterior distributions on the change of stock and flow variables are very similar compared to plugging in an estimate on the aluminium dataset. Therefore, the results presented in the main text use plug in estimate for $\boldsymbol{\tau}$ for faster computation. Details of how $\boldsymbol{\tau}$ and the prior parameters of the change in stock and flow variables are chosen can be found in the supplementary material.

2.4 Posterior predictive checks

For Bayesian modelling of MFA systems, we recommend performing posterior predictive checks to verify whether data generated by the model is similar to the observed data, which gives some assurance that

the prior and model chosen is sensible. Here we briefly describe the method of posterior predictive checking outlined in Chapter 6 of [Gelman et al. \[2013\]](#). Recall that in our model, the observation vector \mathbf{Y} represents the observed data (such as on flows or change in stocks), as well as physical conditions such as mass balance, and $\boldsymbol{\theta}$ the vector of parameters. Let \mathbf{Y}^{rep} be replicated data that could have been observed, the distribution of \mathbf{Y}^{rep} given the observed data \mathbf{Y} , also known as the posterior predictive distribution, is given by:

$$p(\mathbf{Y}^{rep}|\mathbf{Y}) = \int p(\mathbf{Y}^{rep}|\boldsymbol{\theta})p(\boldsymbol{\theta}|\mathbf{Y}) d\boldsymbol{\theta} \quad (22)$$

Typically, the check is done on suitable scalar test quantities $T(\mathbf{Y}, \boldsymbol{\theta})$, chosen based on the real problem being modelled. The test quantity of the replicated data $T(\mathbf{Y}^{rep}, \boldsymbol{\theta})$ is compared with the test quantity of the observed data $T(\mathbf{Y}, \boldsymbol{\theta})$ through statistical tests or graphical checks to look for systematic discrepancies between the simulated and originally observed data. For our Bayesian material flow analysis model, we choose the test quantities to be each individual observed data and mass balance conditions of child processes in the system, in other words we choose test quantities $T_i(\mathbf{Y}, \boldsymbol{\theta}) = Y_i$ for each i . This ensures we minimally check using the posterior predictive distribution that the model is consistent with the existing data as well as mass balance of child processes. One way to compare the observed data with the posterior predictive distribution is to calculate the Bayesian posterior predictive p-values for the test statistic, in our case the marginal observations Y_i , which are given by

$$pval_i = P(Y_i^{rep} \geq Y_i|\mathbf{Y}) = \int \int \mathbb{I}_{Y_i^{rep} \geq Y_i} p(\mathbf{Y}^{rep}|\boldsymbol{\theta})p(\boldsymbol{\theta}|\mathbf{Y}) d\mathbf{Y}^{rep} d\boldsymbol{\theta} \quad (23)$$

Very large or small (e.g. greater than 0.95 or smaller than 0.05) p-value suggests the observed test quantity is unlikely to be replicated in repeated experiments if the model were true, implying there is inconsistency between the model and the data. We also calculate the posterior predictive marginal 95% highest density interval for each $Y_i|\mathbf{Y}$ to see if they contain the observed values Y_i (which include the conservation of mass conditions where $Y_i = 0$).

In practice, the integrals in [Equation \(22\)](#) and [Equation \(23\)](#) are analytically intractable, so we again approximate the posterior predictive distribution via sampling. Specifically we simulate one sample of \mathbf{Y}^{rep} from the posterior predictive distribution for each posterior sample of $\boldsymbol{\theta}$, and we approximate p-values of [Equation \(23\)](#) by checking the proportion of the posterior predictive samples of Y_i^{rep} that exceed the observed value Y_i , for each i .

2.5 Gaussian model

For model comparison purposes and to gain intuition into how Bayesian models perform for MFA problems, it is useful to examine a model with simplified assumptions. In particular, we consider a Gaussian model, where both the prior and the likelihood function are assumed to be normally distributed, and the data is assumed to be linear in terms of $\boldsymbol{\theta}$ (recall from [Section 2.2](#) that the most common forms of MFA data can be expressed linearly in $\boldsymbol{\theta}$):

$$\boldsymbol{\theta} \sim \mathcal{N}(\boldsymbol{\mu}, \Sigma) \quad (24)$$

$$Y_i|\boldsymbol{\theta} \sim \mathcal{N}(\mathbf{x}_i^\top \boldsymbol{\theta}, \tau_i^2) \quad (25)$$

where $\boldsymbol{\mu}$ is the prior mean and Σ is the (positive definite) prior covariance matrix. This gives a mathematically convenient *conjugate* posterior that is also normally distributed, with its posterior mean $\boldsymbol{\mu}^n$ and covariance Σ^n available in closed form:

$$\boldsymbol{\mu}^n = \boldsymbol{\mu} + \Sigma X^\top (X \Sigma X^\top + T)^{-1} (\mathbf{Y} - X \boldsymbol{\mu}) \quad (26)$$

$$\Sigma^n = \Sigma - \Sigma X^\top (X \Sigma X^\top + T)^{-1} X \Sigma \quad (27)$$

where T is a n by n diagonal matrix with entries τ_i^2 , $1 \leq i \leq n$. An advantage of the Gaussian model is that it allows the posterior mean and covariance to be calculated directly without potentially computationally intensive MCMC algorithms. This makes the Gaussian model an easy to compute

baseline to compare with more complicated Bayesian models. Furthermore, owing to the closed form of the posterior, we can bound the mean squared error (MSE) between the posterior mean μ^n and the true parameter (stocks and flows) values θ^* . A discussion on this is provided in the supplementary information, which gives some intuition why Bayesian methods can perform better than non Bayesian methods in the low data setting $n \ll p$.

While computationally convenient, an disadvantage with the Gaussian conjugate model is that the posterior distributions for flow variables can contain non negligible probability on negative values when there is insufficient data or uninformative priors, which is not physically meaningful as flow quantities should be strictly positive, making it not fully Bayesian in this sense. While the posterior mean of the Gaussian model can perform adequately in terms of point estimation, we do not recommend it for uncertainty quantification without very informative priors.

3 Results

In this section we demonstrate our Bayesian MFA method on two different material flow cycles. The first is an aluminium cycle, containing significant disaggregations of processes and flows. We evaluate our model on the aluminium cycle under two different levels of data availability and compare the results. We also use posterior predictive checks to identify inconsistencies between the model and data, and identify processes which are not mass balanced by the available data. The second is a comparatively simpler zinc cycle, which we use to assess the estimation accuracy and uncertainty quantification of our model under varying degrees of prior information and data availability.

3.1 Aluminium cycle data

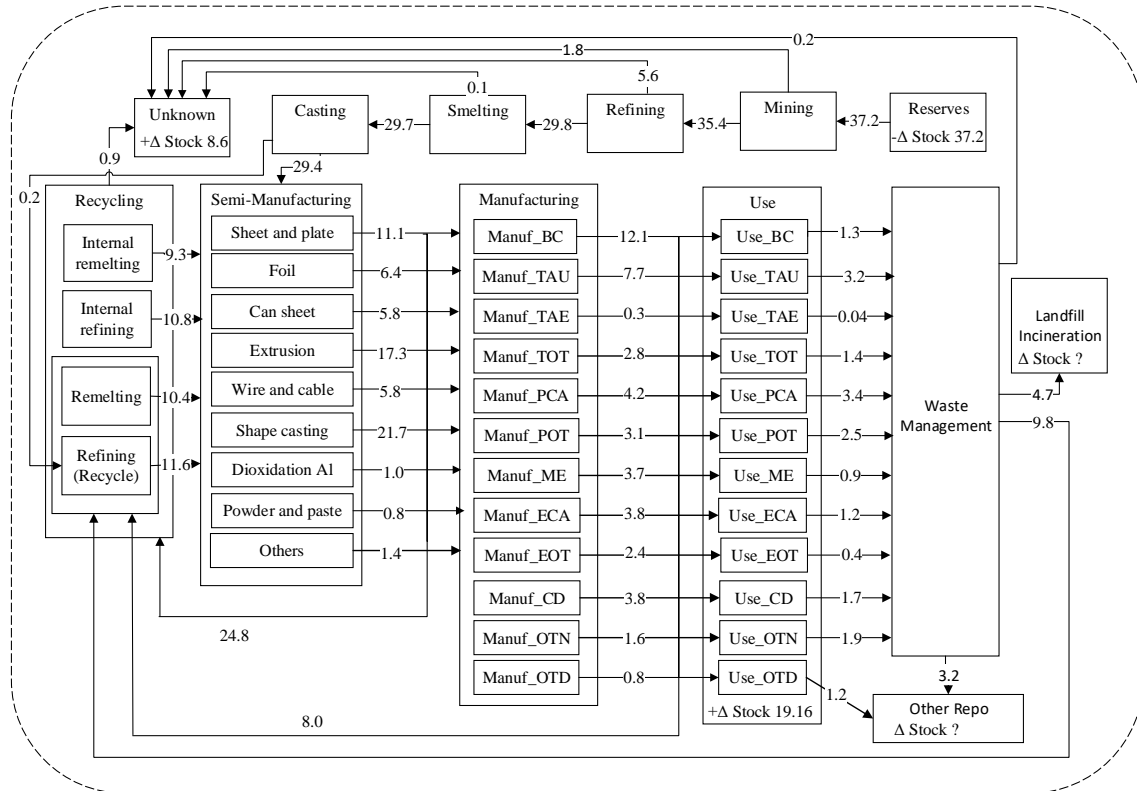


Figure 2: Global anthropogenic metallurgical aluminium cycle in 2009, adapted from Figure 1 of Liu et al. [2013]. Mass of aluminium is measured in megatonnes per year (Mt/yr).

We evaluate our model on the global anthropogenic metallurgical aluminium cycle in 2009 from [Liu et al. \[2013\]](#). The associated system diagram [Figure 2](#) is adapted from Figure 1 of [Liu et al. \[2013\]](#). The aluminium cycle contains significant disaggregations of processes. For example, the ‘Use’ Process contains subprocesses such as ‘Use_BC’ (building and construction) and ‘Use_ME’ (machinery and equipment) representing different use product categories of aluminium.

Furthermore, for aggregated processes such as ‘Manufacturing’ and ‘Recycling’, [Figure 2](#) only displays data on aggregated flows and change in stocks. For example, the flow 12.1 Mt/yr from ‘Manufacturing’ is a combined flow to ‘Use_BC’ and the subprocesses ‘Remelting’ and ‘Refining’ of ‘Recycling’. So it is not clear from [Figure 2](#) alone in what proportion this flow should split among the constituent subprocesses. In tables S5, S6 and S8 of the supplementary information, [Liu et al. \[2013\]](#) provides ratios specifying how certain aggregated flows should split into constituent subflows (known as transfer coefficients), specifically for the aggregate flows from ‘Semi-manufacturing’ to ‘Manufacturing’ and ‘Recycling’, and from ‘Manufacturing’ to ‘Use’ and ‘Recycling’. We evaluate the model under two different scenarios. In scenario A, we deliberately withhold the transfer coefficients in the supplementary information of [Liu et al. \[2013\]](#) from the model, and only use the data displayed in [Figure 2](#). Instead, where transfer coefficients are available to calculate the value of the disaggregated flow, which we will henceforth refer to as the reported value, we set the prior mode of the disaggregated flow variable to the nearest power of 10 of the reported value. Scenario A mimics a situation that could be applicable to many MFA problems, where data is available on the aggregated level but not the disaggregated level, and domain knowledge of the correct order of magnitude of the flows and changes in stock on the disaggregated level is obtained from surveying domain experts, and elicited a weakly informative prior. In scenario B, the same weakly informative prior is used, but the flow ratios in the supplementary information of [Liu et al. \[2013\]](#) are provided to the model as well. Scenario B mimics a situation towards the end of an MFA analysis, when data are available for most of the change in stock and flow variables in the system.

[Figure 3](#) displays a selection of marginal posterior distributions for flow and change in stock variables of disaggregated processes in the aluminium cycle. Only a selection is displayed here for brevity as there are around 180 flow or change in stock variables in the model. Under scenario A, all of the variables’ reported values (when they are available in the supplement of [Liu et al. \[2013\]](#)) are contained within the 95% posterior highest density interval (HDI), though a small number of reported values are near the edge of HDI like the flow ‘ShapeCasting to Manuf_TAU’, which is a disaggregated flow scenario A has no data on. This could be caused by the reported value (around 5.1 Mt/yr) being close to the middle of the nearest orders of magnitudes (1.0 and 10.0 Mt/yr), which is more difficult for a prior based on the nearest order of magnitude (1.0 in this case) to capture without additional data. Under scenario B, the posterior marginal distributions are generally less biased with narrower HDI compared to scenario A, and again the reported values are contained within the 95% posterior HDI. Quantitatively, the average length of the 95% posterior HDI over all change in stock and flow variables under scenario A is 2.3, while under scenario B is 1.6. Overall we can see that reasonably good posterior estimates are obtained under scenario A, which are further improved by the addition of transfer coefficient data in scenario B.

To assess the goodness of fit of our model, we use the method of posterior predictive checking. Here we simulate samples of replicate data and conservation of mass (CoM) conditions from the posterior predictive distribution (PPD) of the model, and compute the marginal posterior predictive 95% HDI and Bayesian p-values to see if the simulated samples of replicate data look plausibly similar compared to the actual observed data, or 0 for CoM conditions. The Bayesian p-value is defined as the probability that replicated data under the posterior predictive distribution is more extreme than the observed data. Extreme p-values (smaller than 0.05 or greater than 0.95, as suggested in [Gelman et al. \[2013\]](#)) suggests the model is inconsistent with the data or CoM conditions. For more detail we refer the reader to the Methods section as well as Chapter 6 of [Gelman et al. \[2013\]](#).

From [Figures 4a, 4b, 4c and 4d](#), it can be seen that the 95% HDIs all contain the observed values for all change in stock data, flow data, conservation of mass conditions and ratio data. Moreover, from [Figures 4e, 4f, 4g and 4h](#), it can be seen that the posterior predictive p-values are mostly between 0.3 and 0.7 and no p-value is smaller than 0.05 or greater than 0.95, suggesting that most p-values are not extreme and the model generally fits the data well. There are a few variables close to extreme values however. In particular, the mass balance for the 6th process ‘Internal remelting’ in [Figure 4g](#) and the 27th flow data in [Figure 4f](#), which represents the total outflow from ‘Internal remelting’ to ‘Semi-manufacturing’ of 9.3 Mt/yr. Upon reviewing the data, it was found the total inflow of ‘Internal remelting’ only summed to

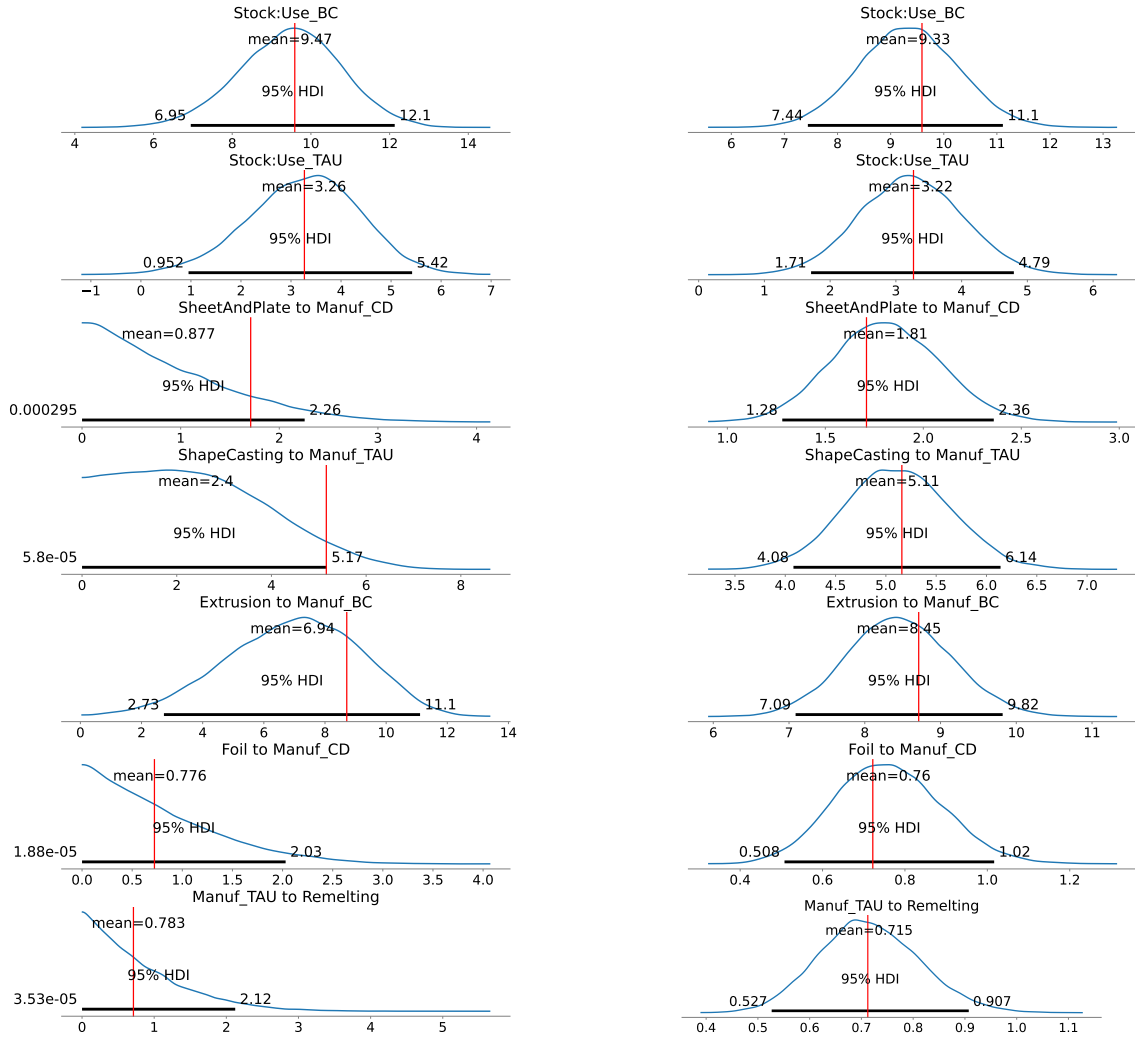


Figure 3: Marginal posterior distributions for a selection of flow and change in stock variables of the aluminium dataset. For each flow or change in stock variables we display both the marginal posterior for scenario A (on the left) and for the scenario B (on the right). Each marginal posterior plot displays the mean and the 95 % highest density interval (HDI). The red vertical line in each graph represents the reported value of the variable, calculated using transfer coefficients provided in the supplement of Liu et al. [2013].

7.1 Mt/yr. The posterior predictive check therefore helpfully highlighted a discrepancy that suggests the data for the process Internal remelting is not mass balanced.

The 13th flow data in Figure 4f, referring to the flow of 0.04 Mt/yr from ‘Use_TAE’ to ‘Wastemanagement’ has a high p-value of around 0.8, which is likely caused by the observed value being extremely small, so replicated data from the model is likely to exceed this value. Similarly, the mass balance for the 16th, 17th and 18th processes in Figure 4g, corresponding to ‘Dioxidation Al’, ‘Powder and paste’ and ‘Others’ respectively have small p-values, likely caused by the flows involving these processes being very small.

In MFA, data is expensive to collect, so it is useful to prioritise which change in stock and flow variables to collect more data on. This will likely depend on what questions the modeller is most interested in answering regarding the real system being modelled. Without specific questions however, Bayesian inference provides default strategies for prioritising which data points to collect, by ranking the variables in terms of descending posterior uncertainty. We plot the top 10 change in stock and flow variables in descending length of their marginal 95% HDI for both scenarios A (Figure 4i) and B (Figure 4j). In scenario B, the most uncertain variables are mostly flows from ‘Casting’ or ‘Recycling’ to

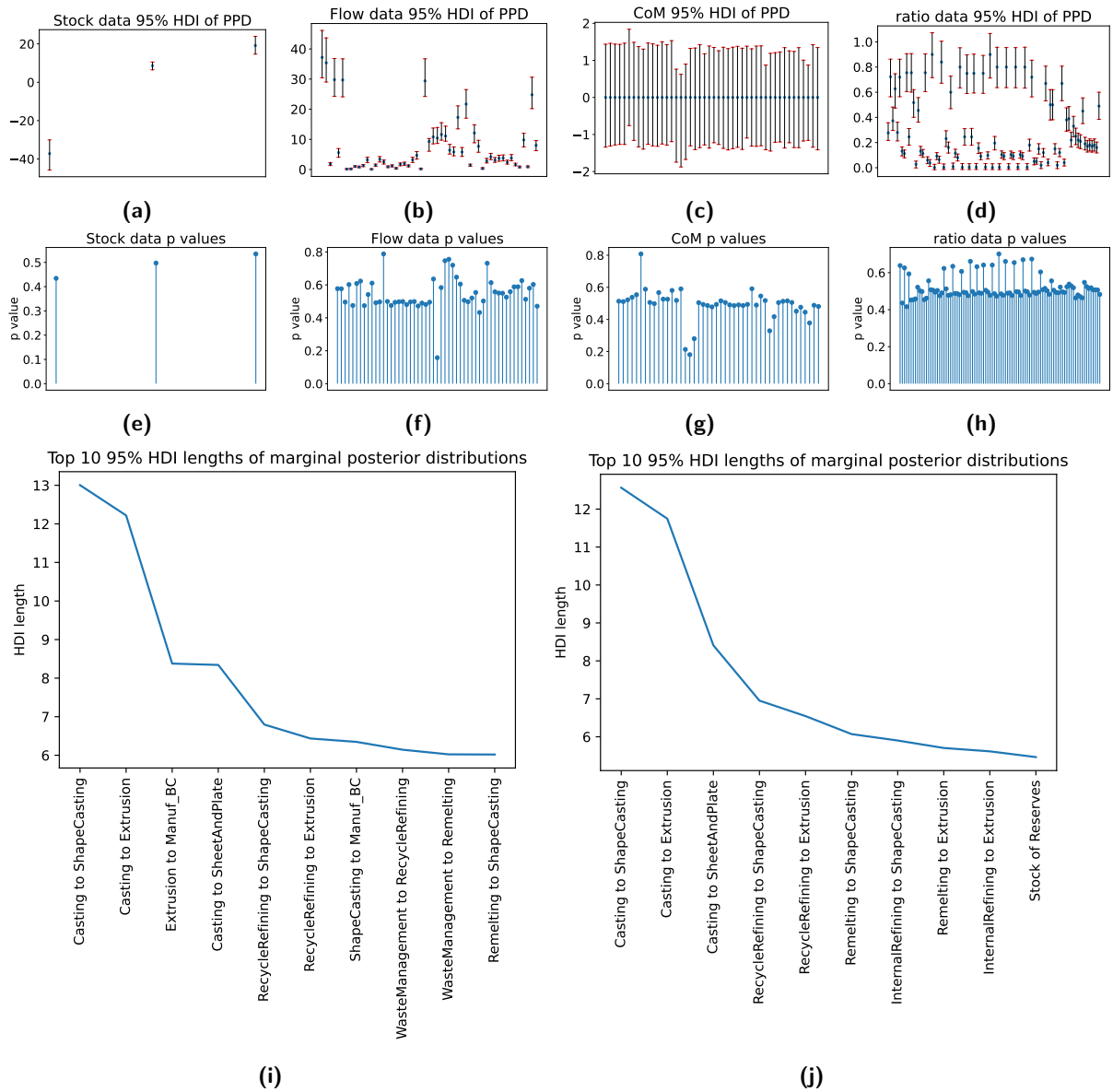


Figure 4: Graphs of posterior predictive checks and posterior HDI lengths, for scenario B. On the first row, we have the sample 95% posterior predictive highest density intervals (red bar) and the observed values (blue dot) for the change in stock data, observed flow data, conservation of mass conditions and flow ratio data respectively. On the second row, we have the posterior predictive p-values for the observed change in stock variables, observed flow variables, conservation of mass conditions and flow ratio data respectively. On the third row, we plot the top 10 largest marginal posterior HDI lengths for scenario A (left), and scenario B (right)

‘Semi-manufacturing’, which is expected as those are the disaggregated flows where data is not available. For scenario A, the most uncertain variables are more scattered throughout the system, as scenario A has no data on any disaggregated flows.

3.2 Zinc cycle Simulation Study

We conduct a simulation study to investigate the estimation accuracy and uncertainty quantification of our model. For this end we consider the zinc cycle in China, ca. 1994-1998, from [Graedel et al. \[2005\]](#). The zinc cycle contains no missing data values, so for the purposes of this simulation, we treat

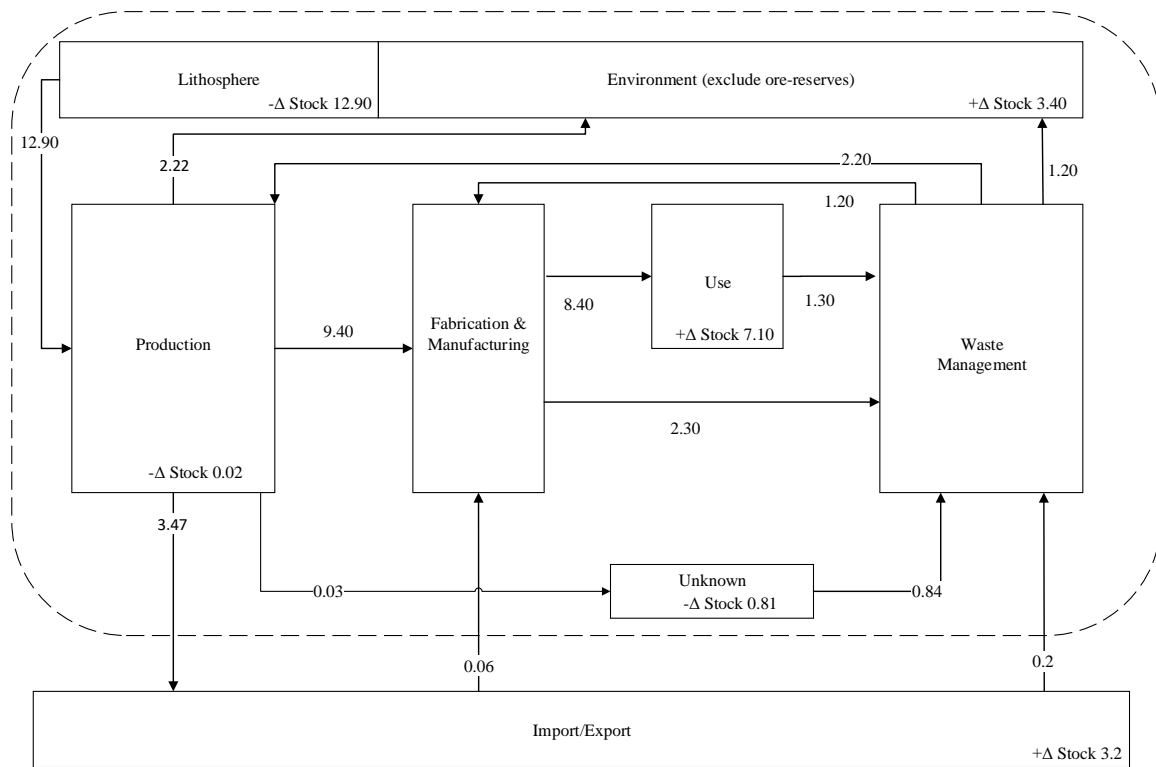


Figure 5: Zinc cycle for China, ca. 1994-1998, adapted from Figure 2d of Graedel et al. [2005]. The unit of mass for zinc is displayed in 10^5 metric tons per year. we explicitly define an ‘Unknown’ Process to account for flows with an unknown source or destination.

the reported data values as the true parameter values of the stock and flow variables. This allows us to assess our model by withholding some data from it and checking the model output against the true values of the stocks and flows. We examine how our model performs in terms of estimation accuracy and uncertainty quantification under different levels of prior knowledge, as data is incrementally added into the model.

To assess estimation accuracy of the model, we calculate how the error of the model evolves as data is randomly added into the model one at a time, starting from no data, until the full dataset becomes available to the model. This process is repeated 50 times and the average error is calculated over the 50 runs. We calculate two types of error, the root mean square error (rmse) and the maximum error, of the model’s predictions compared to the reported values of the change in stocks and flow variables. The posterior mode is taken as the model prediction.

For comparison, we consider several alternate models. First, we consider an alternate Bayesian Gaussian model which has the advantage of a closed form solution, but carries the disadvantage of assigning significant probability to negative values for flow variables in the posterior distribution, which should be strictly positive as negative flows are not physically meaningful. Detail of the Gaussian model is provided in the Methods section. We also provide results from non Bayesian models for comparison, specifically ridge regression and multilayer perceptron (see e.g. Hastie et al. [2001]). In addition, we also investigate the effect of different levels of prior knowledge has on the error. We utilise two different levels of prior knowledge, the first is an ‘uninformative’ prior which sets the prior mode of all variables to the average absolute value of the full data, and the correct sign for change in stock variables. This intuitively represents a prior that knows the average order of magnitude of the system but has little visibility on the individual magnitude of each change in stock or flow. The second is a ‘weakly informative’ prior which sets the prior mode of each change in stock and flow variable to the nearest power of 10 of the true value.

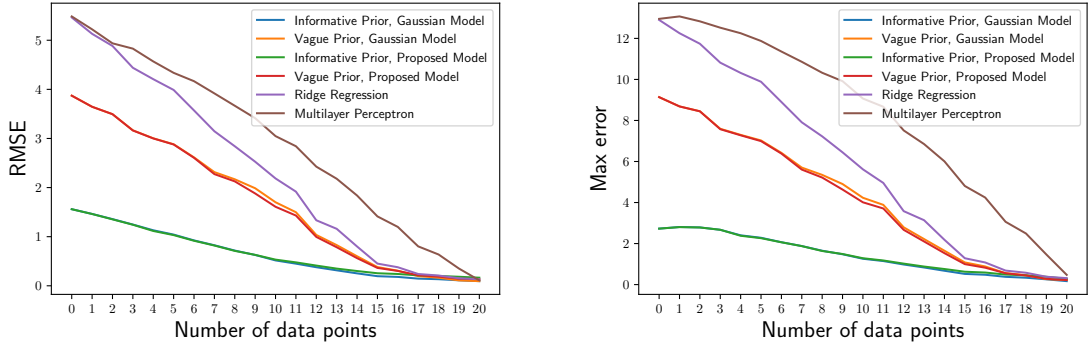


Figure 6: Zinc flow data error analysis: (left) Root mean squared error RMSE of the model plotted against number of data points available to the model, averaged over 50 runs or datasets. (right) Maximum error of the model plotted against the number of data points available to the model, averaged over 50 runs or datasets. For each error type, our model and the Gaussian model are considered under uninformative and informative priors. Ridge regression is provided as a non Bayesian baseline.

This intuitively represents a prior that has knowledge of each flow and change in stock variable to the nearest order of magnitude.

Figure 6 shows the results of our analysis, where the rmse and maximum error of the model are plotted against the number of data points available to the model, averaged over 50 runs. For the non Bayesian models, the starting rmse at no data is around 5.4, whereas for the uninformative prior it is around 4.0 and for the weakly informative prior around 1.5. As data is added, all models exhibit the trend of monotonically decreasing error, but the Bayesian models exhibit noticeably lower error until almost all the data becomes available to the model. Notably, it takes around 10 data points for the uninformative prior models and 12 data points for ridge regression to achieve the starting rsme (around 1.5) of the weakly informative prior model. Therefore, one can consider only knowing the order of magnitude of each flow or change in stock to be roughly equivalent to 10 data points in terms of rmse in this model, demonstrating the utility of being able to incorporate knowledge via a Bayesian prior in such an underdetermined system. For the Gaussian model, theoretical bounds on the mean square error provided in the supplementary material also support the trend exhibited in Figure 6, and the intuition that having an informative prior can greatly increase the model’s accuracy for MFA problems when there is a shortage of data but available expert domain knowledge.

To assess uncertainty quantification of the posterior distribution, we examine whether the 95% posterior marginal highest density intervals (HDIs) of our model have similar level of frequentist coverage, i.e. form correct confidence intervals. The high dimensional nature of MFA models means the dimension of parameter space p (corresponding to the number of flow and change in stock variables in the model) is usually greater or similar in size compared to the number of available data n , and n is typically not large in magnitude. Therefore, results which guarantees asymptotic frequentist coverage of credible regions, such as the Bernstein-von Mises theorem (see e.g. Vaart [1998]), may not apply in MFA problems. We therefore study in simulations the frequentist coverage of our model’s posterior credible intervals, in an effort to understand whether these can be used as reliable confidence intervals. Specifically, we sample 300 sets of the zinc dataset using the likelihood (details of which described in the Methods section). For each dataset sampled, we add data to the model in batches of 5 datapoints at a time (in the order listed from top to bottom in Table 1), and calculate the posterior marginal HDIs to see if they contain the true value for each dataset size $n = 5, 10, 15, 20$. The frequencies of whether the posterior marginal HDIs contain the true value over the 300 runs, known as the coverage probability, are reported in Table 1.

From Table 1, it can be seen that the 95% HDI possess similar levels of coverage probability in most cases. The only notable exception being the uninformative prior at 5 data points, where the coverage probability are close to 0 for the flow variables ‘Lithosphere to Production’ and ‘Production to F& M’, and the change in stock variable for ‘Lithosphere’. This is likely caused by the first 5 data points lacking both the change in stock data and the only flow of ‘Lithosphere’ (to ‘Production’), as well as containing little information on ‘Production’, so the model was unable deduce the true magnitude of how much

Variable Name	Coverage probability(%), average width of 95% HDI							
	Weakly informative prior				Uninformative prior			
	5 data	10 data	15 data	20 data	5 data	10 data	15 data	20 data
Δ Stock: Use	95.3, 3.60	96.3, 3.44	98.0, 3.16	96.3, 3.15	96.0, 3.76	95.3, 3.63	97.7, 3.23	95.7, 3.21
Production to ImportExport	90.7, 3.56	96.3, 3.40	96.7, 3.41	98.0, 2.92	91.3, 3.78	95.7, 3.65	97.7, 3.60	96.0, 3.15
Δ Stock: Environment	98.0, 3.50	97.0, 3.35	97.3, 3.35	98.7, 3.18	95.0, 3.66	97.3, 3.44	96.0, 3.46	98.3, 3.25
WM to Production	94.7, 3.39	96.0, 3.15	96.7, 3.12	93.0, 3.02	94.7, 3.54	94.0, 3.47	94.7, 3.35	91.3, 3.24
ImportExport to WM	100.0, 0.83	100.0, 0.82	100.0, 0.82	100.0, 0.79	96.0, 2.29	99.3, 2.16	97.0, 2.12	98.7, 1.82
Unknown to WM	100.0, 5.07	99.0, 2.48	99.3, 2.18	100.0, 2.19	100.0, 8.52	99.0, 2.53	98.0, 2.42	97.7, 2.48
Lithosphere to Production	100.0, 7.73	96.3, 3.37	95.3, 3.38	93.7, 2.87	0.00, 11.3	96.0, 3.63	94.7, 3.55	94.7, 2.97
Δ Stock: Production	100.0, 0.39	100.0, 0.39	100.0, 0.39	100.0, 0.39	100.0, 16.1	95.0, 3.67	95.3, 3.59	96.0, 3.50
Production to F&M	100.0, 7.69	94.7, 3.32	99.0, 3.19	93.7, 3.06	3.33, 8.25	89.0, 3.55	91.7, 3.39	87.0, 3.21
WM to Environment	100.0, 4.19	98.0, 2.69	98.7, 2.50	99.0, 2.55	100.0, 4.88	96.3, 2.98	97.3, 2.72	95.7, 2.72
F&M to Use	100.0, 7.54	99.7, 7.20	96.3, 3.03	93.0, 2.95	100.0, 9.55	100.0, 9.57	96.3, 3.14	93.3, 3.02
Δ Stock: Unknown	100.0, 6.58	100.0, 4.62	100.0, 2.97	98.7, 2.97	100.0, 13.3	100.0, 7.20	98.0, 3.16	99.3, 3.16
Production to Unknown	100.0, 0.20	100.0, 0.20	100.0, 0.20	100.0, 0.20	100.0, 9.31	97.7, 4.90	93.7, 2.03	96.7, 2.01
F&M to WM	100.0, 6.44	100.0, 6.52	93.3, 3.30	94.3, 3.12	100.0, 10.6	100.0, 11.7	93.3, 3.45	93.7, 3.21
Use to WM	100.0, 5.91	100.0, 5.93	98.3, 2.60	98.0, 2.54	100.0, 7.32	100.0, 7.71	98.0, 2.63	98.7, 2.57
WM to F&M	100.0, 7.79	100.0, 7.29	100.0, 3.79	98.3, 2.63	95.0, 14.1	100.0, 12.4	100.0, 4.16	97.7, 2.74
Δ Stock: ImportExport	97.0, 5.21	99.3, 5.10	99.7, 5.10	96.0, 3.09	84.0, 9.63	90.3, 7.30	95.3, 6.55	93.0, 3.26
Δ Stock: Lithosphere	100.0, 8.21	99.0, 4.95	99.3, 4.95	95.3, 3.04	0.00, 12.2	99.0, 5.24	98.7, 5.18	95.7, 3.11
ImportExport to F&M	100.0, 0.86	100.0, 0.85	100.0, 0.82	100.0, 0.79	100.0, 7.19	100.0, 4.39	100.0, 3.17	98.0, 1.80
Production to Environment	100.0, 3.77	100.0, 3.74	99.3, 3.92	95.0, 2.90	100.0, 4.20	99.0, 3.74	99.7, 4.14	96.0, 2.97

Table 1: Table of coverage probability and average width of 95% highest density intervals (HDI) of the marginal posterior distributions of all flow and change in stock variables in the zinc data under different amounts of data and prior information, computed over 300 runs. Data was added in batches of 5 to the model in the order that they are listed in this table (from top to bottom).

material was taken from the ‘Lithosphere’ with an uninformative prior. On the other hand, the weakly informative prior does not possess this issue as the prior has sufficient coverage over the true value. In addition, the average width of the 95% HDI are generally lower for the weakly informative prior until data for that variable becomes available, which is expected from a more informative prior.

4 Discussion

In this paper, we introduced a novel Bayesian framework that augments traditional MFA by providing point estimation and uncertainty quantification to all stock and flow variables of interest in the system. We demonstrated that our approach can naturally incorporate available domain knowledge of stock and flow variables of interest through the Bayesian prior, and propagate uncertainty in the data through to the posterior distribution from which point estimation and uncertainty quantification of all stock and flow variables of interest can be obtained. We showed that even a weakly informative prior, such as a prior which knows each stock and flow variable to the nearest order of magnitude, is capable of greatly improving the model’s estimation accuracy and quality of its uncertainty quantification, especially during the early stages of the analysis when there is a lack of data, demonstrating the benefit of a Bayesian approach to MFA. Furthermore, unlike previous studies, our Bayesian framework was demonstrated on a system with significant disaggregation of processes and flows, providing posterior distributions on stocks and flows at the lowest level of disaggregation in the system, where data is often unavailable. We also recommend posterior predictive checks on the fitted model for model validation when conducting Bayesian material flow analysis in practice, which offers some assurance that the chosen prior and model is plausible, and can help identify data inconsistencies.

Our Bayesian approach requires prior distributions of all stock and flow variables of interest to be manually elicited, which is an additional requirement compared to non Bayesian methods or more traditional methods of MFA. However, we argue that this should be an important and standard part of any material flow analysis, where domain knowledge is generally available and should be continuously collated, and the prior distribution offers a convenient mathematical way of incorporating this knowledge into the model. The Bayesian approach also inevitably comes with a higher computational cost, as the full posterior distribution of each variable of interest needs to be calculated rather than just a point estimate, and may run into convergence issues [Betancourt \[2017\]](#). The No-U-Turn Sampler HMC algorithm used for our model took around 20 minutes to generate 20000 posterior samples for the aluminium dataset, which we consider acceptable. Furthermore, convergence diagnostic checks suggests posterior samples from the model are valid (details can be found in the supplementary information). We also note that most MFA literature do not use very large datasets so we do not anticipate computational cost to be a major issue for most MFA studies. However, for much larger material flow datasets, approximate methods such as variational Bayes can be employed to reduce the computational cost, or minimally just estimating the posterior mode directly (and forgoing uncertainty quantification) can potentially yield better point estimates than a non Bayesian method if informative priors are available.

Acknowledgements This work was supported by the UKRI Interdisciplinary Circular Economy Centre For Mineral-based Construction Materials under the EPSRC Grant EP/V011820/1. The authors are grateful to Mohit Arora, Nicola Gambaro, Ugo Legendre and Shen Zhenxia for useful discussions.

References

- United nations resource management system: An overview of concepts, objectives and requirements (ece energy series no. 68), 2020. URL <https://unece.org/sustainable-energy/publications/united-nations-resource-management-system-overview-concepts>.
- World population prospects - population division, 2022. URL <https://population.un.org/wpp/>.
- M. Bertram, K. J. Martchek, and G. Rombach. Material flow analysis in the aluminum industry. *Journal of Industrial Ecology*, 13(5):650–654, 2009. doi: <https://doi.org/10.1111/j.1530-9290.2009.00158.x>. URL <https://onlinelibrary.wiley.com/doi/abs/10.1111/j.1530-9290.2009.00158.x>.
- M. Betancourt. A conceptual introduction to hamiltonian monte carlo. 2017. doi: 10.48550/ARXIV.1701.02434. URL <https://arxiv.org/abs/1701.02434>.
- P. H. Brunner and H. Rechberger. Practical handbook of material flow analysis. *The International Journal of Life Cycle Assessment*, 9(5):337–338, Sep 2004. ISSN 1614-7502. doi: 10.1007/BF02979426. URL <https://doi.org/10.1007/BF02979426>.
- O. Cencic and R. Frühwirth. A general framework for data reconciliation—part i: Linear constraints. *Computers & Chemical Engineering*, 75:196–208, 2015.

- ISSN 0098-1354. doi: <https://doi.org/10.1016/j.compchemeng.2014.12.004>. URL <https://www.sciencedirect.com/science/article/pii/S0098135414003330>.
- O. Cencic and R. Frühwirth. Data reconciliation of nonnormal observations with nonlinear constraints. *Journal of Applied Statistics*, 45(13):2411–2428, 2018. doi: 10.1080/02664763.2017.1421916. URL <https://doi.org/10.1080/02664763.2017.1421916>.
- J. M. Cullen, J. M. Allwood, and M. D. Bambach. Mapping the global flow of steel: From steelmaking to end-use goods. *Environmental Science & Technology*, 46(24):13048–13055, Dec 2012. ISSN 0013-936X. doi: 10.1021/es302433p. URL <https://doi.org/10.1021/es302433p>.
- D. da Costa Reis, Y. Mack-Vergara, and V. M. John. Material flow analysis and material use efficiency of brazil’s mortar and concrete supply chain. *Journal of Industrial Ecology*, 23(6):1396–1409, 2019. doi: <https://doi.org/10.1111/jiec.12929>. URL <https://onlinelibrary.wiley.com/doi/abs/10.1111/jiec.12929>.
- J. Dong, J. Liao, X. Huan, and D. Cooper. Expert elicitation and data noise learning for material flow analysis using bayesian inference, 2022. URL <https://arxiv.org/abs/2207.09288>.
- M. Fischer-Kowalski, F. Krausmann, S. Giljum, S. Lutter, A. Mayer, S. Bringezu, Y. Moriguchi, H. Schütz, H. Schandl, and H. Weisz. Methodology and indicators of economy-wide material flow accounting. *Journal of Industrial Ecology*, 15(6):855–876, 2011. doi: <https://doi.org/10.1111/j.1530-9290.2011.00366.x>. URL <https://onlinelibrary.wiley.com/doi/abs/10.1111/j.1530-9290.2011.00366.x>.
- A. Gelman, J. Carlin, H. Stern, D. Dunson, A. Vehtari, and D. Rubin. *Bayesian Data Analysis, Third Edition*. Chapman and Hall/CRC, 2013. ISBN 9781439840955.
- F. Gottschalk, R. W. Scholz, and B. Nowack. Probabilistic material flow modeling for assessing the environmental exposure to compounds: Methodology and an application to engineered nano-tio2 particles. *Environmental Modelling & Software*, 25(3):320–332, 2010. ISSN 1364-8152. doi: <https://doi.org/10.1016/j.envsoft.2009.08.011>. URL <https://www.sciencedirect.com/science/article/pii/S1364815209002394>.
- T. E. Graedel, D. van Beers, M. Bertram, K. Fuse, R. B. Gordon, A. Gritsinin, E. M. Harper, A. Kapur, R. J. Klee, R. Lifset, L. Memon, and S. Spatari. The multilevel cycle of anthropogenic zinc. *Journal of Industrial Ecology*, 9(3):67–90, 2005. doi: <https://doi.org/10.1162/1088198054821573>. URL <https://onlinelibrary.wiley.com/doi/abs/10.1162/1088198054821573>.
- T. Hastie, R. Tibshirani, and J. Friedman. *The Elements of Statistical Learning*. Springer Series in Statistics. Springer New York Inc., New York, NY, USA, 2001.
- A. E. Hoerl and R. W. Kennard. Ridge regression: Biased estimation for nonorthogonal problems. *Technometrics*, 42(1):80–86, 2000. ISSN 00401706. URL <http://www.jstor.org/stable/1271436>.
- M. Hoffman and A. Gelman. The no-u-turn sampler: Adaptively setting path lengths in hamiltonian monte carlo. *Journal of Machine Learning Research*, 15:1953–1623, 2014.
- S. M. Jowitt. COVID-19 and the Global Mining Industry. *SEG Discovery*, (122):33–41, 07 2020. ISSN 1550-297X. doi: 10.5382/SEGnews.2020-122.fea-02. URL <https://doi.org/10.5382/SEGnews.2020-122.fea-02>.
- S. M. Jowitt, G. M. Mudd, and J. F. H. Thompson. Future availability of non-renewable metal resources and the influence of environmental, social, and governance conflicts on metal production. *Nature News*, Sep 2020. URL <https://www.nature.com/articles/s43247-020-0011-0>.
- S. Koermer and A. Noble. The utility of bayesian data reconciliation for separations. *Minerals Engineering*, 169:106837, 2021. ISSN 0892-6875. doi: <https://doi.org/10.1016/j.mineng.2021.106837>. URL <https://www.sciencedirect.com/science/article/pii/S0892687521000662>.
- J. K. Kruschke. *Doing Bayesian Data Analysis: A tutorial with R, Jags, and Stan*. Academic Press, 2015.
- J. C. Lederer. *Fundamentals of high-dimensional statistics: With exercises and R labs*. Springer Texts in Statistics. Springer, 1 edition, 2022.
- G. Liu, C. E. Bangs, and D. B. Müller. Stock dynamics and emission pathways of the global aluminium cycle. *Nature Climate Change*, 3(4):338–342, Apr 2013. ISSN 1758-6798. doi: 10.1038/nclimate1698. URL <https://doi.org/10.1038/nclimate1698>.
- R. C. Lupton and J. M. Allwood. Incremental material flow analysis with bayesian inference. *Journal of Industrial Ecology*, 22(6):1352–1364, 2018. doi: <https://doi.org/10.1111/jiec.12698>. URL <https://onlinelibrary.wiley.com/doi/abs/10.1111/jiec.12698>.

- K. Matsubae-Yokoyama, H. Kubo, K. Nakajima, and T. Nagasaka. A material flow analysis of phosphorus in japan. *Journal of Industrial Ecology*, 13(5):687–705, 2009. doi: <https://doi.org/10.1111/j.1530-9290.2009.00162.x>. URL <https://onlinelibrary.wiley.com/doi/abs/10.1111/j.1530-9290.2009.00162.x>.
- A. Miatto, H. Schandl, T. Fishman, and H. Tanikawa. Global patterns and trends for non-metallic minerals used for construction. *Journal of Industrial Ecology*, 21(4):924–937, 2017. doi: <https://doi.org/10.1111/jiec.12471>. URL <https://onlinelibrary.wiley.com/doi/abs/10.1111/jiec.12471>.
- L. Mirsky. A trace inequality of john von neumann. *Monatshefte für Mathematik*, 79(4):303–306, Dec 1975. ISSN 1436-5081. doi: 10.1007/BF01647331. URL <https://doi.org/10.1007/BF01647331>.
- G. M. Mudd. Assessing the availability of global metals and minerals for the sustainable century: From aluminium to zirconium. *Sustainability*, 13(19), 2021. ISSN 2071-1050. doi: 10.3390/su131910855. URL <https://www.mdpi.com/2071-1050/13/19/10855>.
- R. Myers, B. Reck, and T. Graedel. Ystafdb, a unified database of material stocks and flows for sustainability science. *Scientific Data*, 6, 2019a. doi: 10.1038/s41597-019-0085-7. URL <http://dx.doi.org/10.1038/s41597-019-0085-7>.
- R. J. Myers, T. Fishman, B. K. Reck, and T. E. Graedel. Unified materials information system (umis): An integrated material stocks and flows data structure. *Journal of Industrial Ecology*, 23(1):222–240, 2019b. doi: <https://doi.org/10.1111/jiec.12730>. URL <https://onlinelibrary.wiley.com/doi/abs/10.1111/jiec.12730>.
- J. Salvatier, T. V. Wiecki, and C. Fonnesbeck. Probabilistic programming in python using PyMC3. *PeerJ Computer Science*, 2:e55, apr 2016. doi: 10.7717/peerj-cs.55. URL <https://doi.org/10.7717/peerj-cs.55>.
- R. Tibshirani. Regression shrinkage and selection via the lasso. *Journal of the Royal Statistical Society. Series B (Methodological)*, 58(1):267–288, 1996. ISSN 00359246. URL <http://www.jstor.org/stable/2346178>.
- A. W. v. d. Vaart. *Asymptotic Statistics*. Cambridge Series in Statistical and Probabilistic Mathematics. Cambridge University Press, 1998. doi: 10.1017/CBO9780511802256.
- C. D. Westbroek, J. Bitting, M. Craglia, J. M. C. Azevedo, and J. M. Cullen. Global material flow analysis of glass: From raw materials to end of life. *Journal of Industrial Ecology*, 25(2):333–343, 2021. doi: <https://doi.org/10.1111/jiec.13112>. URL <https://onlinelibrary.wiley.com/doi/abs/10.1111/jiec.13112>.

A Supplementary Information

A.1 Parent and child processes

In this section we elaborate on the parent and child process framework used to model disaggregation of processes or flows in MFA systems, and provide a simple illustrative example. Recall that a child process is any process which does not contain subprocesses, and a parent process is any process which does contain subprocesses. This by definition partitions all processes in the system into either child or parent processes, and all parent processes can be broken down into a set of constituent child processes. This partition of parent and child processes is useful because it allows multiple levels of disaggregation to be modelled using just two types of processes with a bottom up approach. In particular, only the child processes need to be modelled, and the parent processes variables are simply the sum of its constituent child processes variables. To illustrate this, consider the (non mass conserved) simple example of [Figure 7](#):

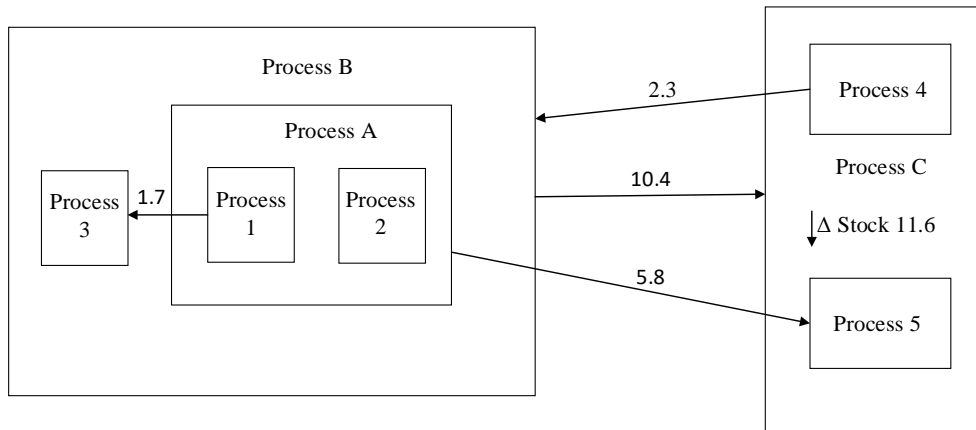


Figure 7: A simple example of a MFA system with aggregation

From a typical top down approach, this example system contains 3 levels of disaggregation, since ‘Process B’ contains ‘Process A’, and ‘Process A’ in turn contains ‘Process 1’ and ‘Process 2’. In our framework however, the child processes are ‘Process 1’, ‘Process 2’, ‘Process 3’, ‘Process 4’ and ‘Process 5’ while the parent processes are ‘Process A’, ‘Process B’ and ‘Process C’. The data in [Figure 7](#) are the flows $U_{1,3} = 1.7$, $U_{4,B} = 2.3$, $U_{B,C} = 10.4$ and $U_{A,5} = 5.8$, and the change of stock $S_C = 11.6$. The change in stock or flow data involving parent or aggregated processes can all be expressed in terms of flows involving child processes:

$$S_C = S_4 + S_5 \tag{28}$$

$$U_{4,B} = U_{4,1} + U_{4,2} + U_{4,3} \tag{29}$$

$$U_{B,C} = U_{1,4} + U_{2,4} + U_{3,4} + U_{1,5} + U_{2,5} + U_{3,5} \tag{30}$$

$$U_{A,5} = U_{1,5} + U_{2,5} \tag{31}$$

The data in this example can therefore be formulated with the following design matrix:

$$\begin{pmatrix} 0 & 0 & 1 & 0 & 0 & 0 & 0 & 0 & 0 & 0 & 0 & 0 & 0 \\ 1 & 1 & 0 & 0 & 0 & 0 & 0 & 0 & 0 & 0 & 0 & 0 & 0 \\ 0 & 0 & 0 & 0 & 0 & 0 & 0 & 0 & 0 & 1 & 1 & 1 & 1 \\ 0 & 0 & 0 & 1 & 1 & 1 & 1 & 1 & 1 & 0 & 0 & 0 & 0 \\ 0 & 0 & 0 & 0 & 1 & 0 & 1 & 0 & 0 & 0 & 0 & 0 & 0 \end{pmatrix} \begin{pmatrix} S_4 \\ S_5 \\ U_{1,3} \\ U_{1,4} \\ U_{1,5} \\ U_{2,4} \\ U_{2,5} \\ U_{3,4} \\ U_{3,5} \\ U_{4,1} \\ U_{4,2} \\ U_{4,3} \end{pmatrix} = \begin{pmatrix} 1.7 \\ 11.6 \\ 2.3 \\ 10.4 \\ 5.8 \end{pmatrix} \tag{32}$$

A.2 Model diagnostics

In this section we present trace plots for a selection of change in stock and flow variables in the aluminium model, in order to check the convergence of the No-U-Turn Sampler Hamiltonian Monte Carlo algorithm. Using the No-U-Turn Sampler, we sampled 2 independent chains of 12000 samples, with the first 2000 samples used for tuning and discarded from the final posterior samples. The tuning samples are to give the Markov Chains iterations to converge to the target posterior distribution before extracting samples to approximate the posterior distribution. The traceplots in [Figure 8](#) suggests both chains have converged to the same distribution. Furthermore, for both scenario A and scenario B, the Gelman-Rubin diagnostic statistic (see for example Chapter 11 of [Gelman et al. \[2013\]](#)) for all change in stock and flow variables in the model have converged to 1.0 and no divergences were reported, indicating the posterior samples are reliable ([Betancourt \[2017\]](#)).

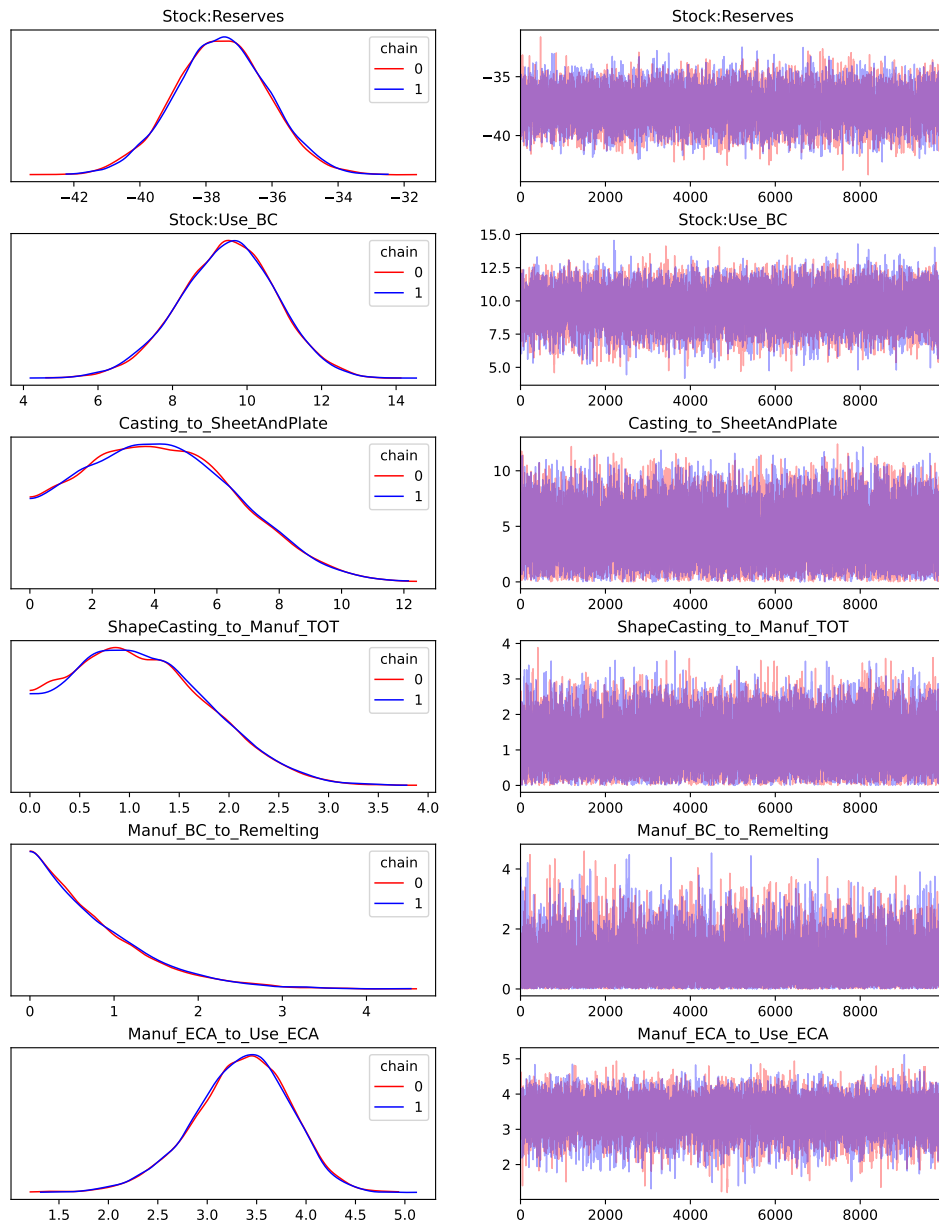


Figure 8: Traceplots for a selection of change in stock and flow variables in the aluminium model, scenario A.

A.3 Detail of prior parameters for the aluminium model

In this section we give detail on the choice of prior parameters for the model evaluation of the aluminium dataset, A summary of the parameter values described in this section can be found in [Table 3](#). Below we describe and motivate the choices:

The prior mode μ_i or $\mu_{j,k}$ of change in stock or flow variables respectively are chosen to be equal to the nearest power of 10 of the reported value when it is available. For example, the flow from ‘Mining’ to ‘Refining’ with a reported value 35.4 Mt/yr is assigned a prior mode of $\mu_{1,2} = 10.0$ Mt/yr. If the flow or change in stock variable has no reported value, it is assigned an uninformative prior mode of 1.0 Mt/yr instead.

The prior standard deviation σ_i for the change in stock variables are chosen to be $\sigma_i = \max(\sqrt{40}\mu_i, 0.1)$, or 10.0 if there is no reported value for the change in stock or flow variable. The corresponding parameter $\sigma_{j,k}$ for the flow variables are chosen similarly. For example, $\sigma_{1,2} = \sqrt{40} * 10.0 = 63.25$ for the flow from ‘Mining’ to ‘Refining’. This choice is motivated by when μ_i is specified to the correct order of magnitude, the true value of the variable is at most $4.5\mu_i$ away, and so σ_i is chosen on a similar scale. The maximum here is to ensure a minimum prior standard deviation of 0.1.

The overall rationale of this choice for the prior distribution is to elicit a weakly informative prior distribution with a prior mode that captures the order of magnitude of the change in stock or flow, coupled with a relatively large prior variance, in order to reflect a realistic baseline of domain knowledge to aim for when conducting MFA.

For lack of better information, the standard deviation parameters for change in stock data noise $\tau_{i'}$ are chosen to be $\tau_{i'} = \max(0.1Y_{i'}, 0.1)$, where $Y_{i'}$ are the observed change in stock data. The corresponding parameters $\tau_{j'}$ for flow data noise is chosen similarly. In other words, the data standard deviation is equal to 10% of the observed data as in [Lupton and Allwood \[2018\]](#), but with a minimum of 0.1 to account for a minimum degree of uncertainty from rounding or other measurement errors. For the ratio data noise, the standard deviation parameters $\tau_{k'}$ are chosen with a somewhat smaller minimum $\tau_{k'} = \max(0.1Y_{k'}, 0.01)$, where $Y_{k'}$ is the observed ratio.

We also ran the model assigning an Inverse Gamma prior to the standard deviation parameters of the data rather than the plug in values described in the previous paragraph. The hyperparameters of the Inverse Gamma prior for the change in stock data $a_{i'}$ and $b_{i'}$ are chosen as $a_{i'} = 4.0$ and $b_{i'} = 3 \max(0.1Y_{i'}, 0.1)$, which sets the prior mean to the plug in values $\max(0.1Y_{i'}, 0.1)$ in the previous paragraph. The hyperparameters for the flow and flow ratio data are chosen similarly. However, it was found this increased computational time by about 50% while only extremely marginal decreases to the posterior uncertainty of the stock and flow variables were observed. For example, in scenario A, the average posterior marginal 95% HDI of all change in stock and flow variables decreased from 2.31 to 2.28, so we simply used the plug in values for the results presented in the main text of the paper.

For the mass conservation conditions, a small constant standard deviation of $\tau_{l'} = 0.5$ is chosen for all processes.

Parameter	Parameter prior value
μ_i	nearest power of 10 of reported value, or 1.0 if unavailable
$\mu_{j,k}$	nearest power of 10 of reported value, or 1.0 if unavailable
σ_i	$\max(\sqrt{40}\mu_i, 0.1)$, or 10.0 if reported value is unavailable
$\sigma_{j,k}$	$\max(\sqrt{40}\mu_{j,k}, 0.1)$, or 10.0 if reported value is unavailable
$\tau_{i'}$	$\max(0.1Y_{i'}, 0.1)$
$\tau_{j'}$	$\max(0.1Y_{j'}, 0.1)$
$\tau_{k'}$	$\max(0.1Y_{k'}, 0.01)$
$\tau_{l'}$	0.5
$a_{i'}$	4.0
$b_{i'}$	$3 \max(0.1Y_{i'}, 0.1)$
$a_{j'}$	4.0
$b_{j'}$	$3 \max(0.1Y_{j'}, 0.1)$
$a_{k'}$	4.0
$b_{k'}$	$3 \max(0.1Y_{k'}, 0.01)$

Table 2: Table of parameters for the aluminium model

A.4 Detail of prior parameters for the zinc model

In this section we give detail on how the prior parameters were chosen for the zinc model. Recall that we considered two different priors for the zinc model, an uninformative prior and a weakly informative prior. For the uninformative prior, the prior modes μ_i of the change in stock variables are chosen to be 3.6575 (measured in 10^5 tonnes/Yr), equal to the mean of the absolute value of all the stocks and flow variables in the data, to represent a prior that only has a rough knowledge of the average order of magnitude of the system, but not the order of magnitude of each individual stock or flow. For weakly informative prior, μ_i are chosen the same way as the aluminium case, where the prior mode is set to the nearest power of 10 of the ‘true’ reported value. The prior standard deviation parameters σ_i are chosen to be a constant $\sqrt{40}$ in the uninformative case, and $\sigma_i = \max(\min(4\mu_i, 4), 0.1)$ in the weakly informative case. Like in the aluminium model, σ_i for the weakly informative prior is chosen at a similar scale compared to $4.5\mu_i$ but somewhat smaller and capped at a maximum of 4.0 to reflect the fact that the size of flows are relatively smaller in the zinc data (when measured in 10^5 tonnes/Yr, compared to the aluminium data which is measured in Mt/yr). The corresponding prior parameters for the flow variables $\mu_{j,k}$ and $\sigma_{j,k}$ are chosen similarly.

The noise standard deviation parameters of the observed data is chosen to be a constant $\tau = 1.0$ throughout for all data, and similarly for the mass conservation conditions. Here the noise parameters are chosen to be somewhat larger than the aluminium model to speed up the computation of the No-U-Turn Sampler MCMC algorithm, as the model needed to be computed 2400 times over the varying degrees of prior knowledge and available data to generate the coverage probability results in Table 1 of the main text. In particular, small values of the noise parameter induces high curvature which makes the sampling algorithm take longer to explore the posterior distribution. Similarly, for assessing point estimation (root mean squared error and maximum error) of the model on the zinc data, the posterior mode of the model is estimated directly via optimisation for faster computational speed, rather than through approximating the entire posterior distribution using MCMC.

Parameter	Parameter prior value (weakly informative prior)	Parameter prior value (uninformative prior)
μ_i	nearest power of 10 of reported value	± 3.6575 (sign depending if the change in stock is positive or negative)
$\mu_{j,k}$	nearest power of 10 of reported value	3.6575
σ_i	$\max(\min(4\mu_i, 4), 0.1)$	$\sqrt{40}$
$\sigma_{j,k}$	$\max(\min(4\mu_{j,k}, 4), 0.1)$	$\sqrt{40}$
τ	1.0	1.0

Table 3: Table of parameters for the zinc model

A.5 Theoretical mean squared error bound on the Gaussian model

In this section we provide some theoretical analysis for the mean squared error of the Gaussian model. While the Gaussian model is a model with simplified assumptions and not the main model we advocate for MFA, it gives some intuition into why Bayesian methods perform better than non Bayesian methods in the low data setting $n \ll p$.

Owing to the closed form of the posterior of the Gaussian model described in the Methods section of the main text, we can bound the mean squared error (MSE) between the posterior mean $\boldsymbol{\mu}^n$ and the true parameter (stocks and flows) values $\boldsymbol{\theta}^*$ as follows:

Theorem 1. *Let $\tau_i^2 = \tau^2$, in other words $T = \tau^2 I$, I the identity matrix. The mean squared error between the posterior mean of the Gaussian posterior $\boldsymbol{\mu}^n$ and the true stock and flow values $\boldsymbol{\theta}^*$ can be bounded above in the following way:*

$$\begin{aligned} \mathbb{E}(\|\boldsymbol{\theta}^* - \boldsymbol{\mu}^n\|_2^2) &= \mathbb{E}\left(\sum_{j=1}^p (\theta_j^* - \mu_j^n)^2\right) \\ &\leq \text{Tr}(\Sigma^{-1/2}(\boldsymbol{\theta}^* - \boldsymbol{\mu})(\boldsymbol{\theta}^* - \boldsymbol{\mu})^\top \Sigma^{-1/2}) \lambda_1(p - n + \sum_{j=1}^n \frac{\tau^4}{(d_j^2 + \tau^2)^2}) + \tau^2 \sum_{j=1}^n \frac{\lambda_1 d_j^2}{(d_j^2 + \tau^2)^2} \end{aligned} \quad (33)$$

where $\lambda_1 \geq \lambda_2 \geq \dots \geq \lambda_p > 0$ are the eigenvalues of Σ in descending order, and $d_1 \leq d_2 \leq \dots \leq d_n$ are the singular values of $X\Sigma^{1/2}$ in ascending order.

The bound in Equation (33) helps to give some insight into how the mean squared error of the model evolves as more data is added. This is perhaps easiest to see in the case when τ is near 0 (meaning the data is almost noiseless), which leaves

$$\text{Tr}(\Sigma^{-1/2}(\boldsymbol{\theta}^* - \boldsymbol{\mu})(\boldsymbol{\theta}^* - \boldsymbol{\mu})^\top \Sigma^{-1/2}) \lambda_1(p - n)$$

as the dominant term. The $\text{Tr}(\Sigma^{-1/2}(\boldsymbol{\theta}^* - \boldsymbol{\mu})(\boldsymbol{\theta}^* - \boldsymbol{\mu})^\top \Sigma^{-1/2})$ part of this term can be interpreted as a measurement of how close the prior mean is to the true values of the parameters (it is 0 when $\boldsymbol{\theta}^* = \boldsymbol{\mu}$) and does not depend on the data, while the factor $\lambda_1(p - n)$ decreases as n increases, meaning as more data is added. This indicates that in a high dimensional setting $n \ll p$ which is inherent in MFA studies, the availability of informative priors is key to obtaining more accurate estimates of the true stock and flow values.

Furthermore, in the case when $\Sigma = \lambda_1 I$, Equation (33) can be directly compared with the ridge regression case. Since ridge regression is equivalent to the case when $\boldsymbol{\mu} = \mathbf{0}$ and $\Sigma = \lambda_1 I$, Equation (33) is smaller for the Gaussian model compared to ridge regression whenever $\text{Tr}((\boldsymbol{\theta}^* - \boldsymbol{\mu})(\boldsymbol{\theta}^* - \boldsymbol{\mu})^\top) = \|\boldsymbol{\theta}^* - \boldsymbol{\mu}\|_2^2$ is smaller than $\|\boldsymbol{\theta}^*\|_2^2$. In other words whenever the prior mean $\boldsymbol{\mu}$ is closer to the true value in (L2) distance than the zero vector $\mathbf{0}$, which is consistent with the simulations presented in the Results section of the main text.

Proof of Theorem 1.

Recall that the posterior mean of the conjugate Gaussian model can be written as:

$$\boldsymbol{\mu}^n = \boldsymbol{\mu} + \Sigma X^\top (X \Sigma X^\top + \tau^2 I)^{-1} (X(\boldsymbol{\theta}^* - \boldsymbol{\mu}) + \boldsymbol{\epsilon})$$

This can be derived from looking at the joint distribution $[\boldsymbol{\theta}, X\boldsymbol{\theta} + \boldsymbol{\epsilon}]^\top$ and using standard Gaussian conditioning formulae:

$$\begin{bmatrix} \boldsymbol{\theta} \\ X\boldsymbol{\theta} + \boldsymbol{\epsilon} \end{bmatrix} \sim \mathcal{N}\left(\begin{bmatrix} \boldsymbol{\mu} \\ X\boldsymbol{\mu} \end{bmatrix}, \begin{bmatrix} \Sigma & \Sigma X^\top \\ X\Sigma & X\Sigma X^\top + \tau^2 I \end{bmatrix}\right) \quad (34)$$

Suppose $\dim(X) = (n, p)$, $\dim(\Sigma) = (p, p)$, $\dim(\boldsymbol{\mu}) = \dim(\boldsymbol{\theta}^*) = (p, 1)$, $\dim(\boldsymbol{\epsilon}) = (n, 1)$, and we'll assume $n < p$, since material flow analysis typically has less data than parameters. Assume Σ is symmetric positive definite and X has full rank. The mean squared error (MSE) between the posterior mean $\boldsymbol{\mu}^n$ and the true value $\boldsymbol{\theta}^*$ is equal to:

$$\begin{aligned}
MSE &= \mathbb{E} \|\boldsymbol{\theta}^* - \boldsymbol{\mu} - \Sigma X^\top (X \Sigma X^\top + \tau^2 I)^{-1} (X(\boldsymbol{\theta}^* - \boldsymbol{\mu}) + \boldsymbol{\epsilon})\|_2^2 \\
&= \mathbb{E} (\boldsymbol{\beta} - \Sigma X^\top (X \Sigma X^\top + \tau^2 I)^{-1} (X \boldsymbol{\beta} + \boldsymbol{\epsilon}))^\top (\boldsymbol{\beta} - \Sigma X^\top (X \Sigma X^\top + \tau^2 I)^{-1} (X \boldsymbol{\beta} + \boldsymbol{\epsilon})) \\
&= \mathbb{E} (\boldsymbol{\beta}^\top (I - \Sigma X^\top (X \Sigma X^\top + \tau^2 I)^{-1} X)^\top (I - \Sigma X^\top (X \Sigma X^\top + \tau^2 I)^{-1} X) \boldsymbol{\beta}) \\
&\quad + \mathbb{E} (\boldsymbol{\epsilon}^\top (\Sigma X^\top (X \Sigma X^\top + \tau^2 I)^{-1})^\top \Sigma X^\top (X \Sigma X^\top + \tau^2 I)^{-1} \boldsymbol{\epsilon})
\end{aligned}$$

Where $\boldsymbol{\beta} = \boldsymbol{\theta}^* - \boldsymbol{\mu}$. At this point we decompose the MSE into the bias and variance terms. Let

$$MSE_1 = \mathbb{E} (\boldsymbol{\beta}^\top (I - \Sigma X^\top (X \Sigma X^\top + \tau^2 I)^{-1} X)^\top (I - \Sigma X^\top (X \Sigma X^\top + \tau^2 I)^{-1} X) \boldsymbol{\beta})$$

denote the bias term. and

$$MSE_2 = \mathbb{E} (\boldsymbol{\epsilon}^\top (\Sigma X^\top (X \Sigma X^\top + \tau^2 I)^{-1})^\top \Sigma X^\top (X \Sigma X^\top + \tau^2 I)^{-1} \boldsymbol{\epsilon})$$

denote the variance term.

For the bias term, using the fact that the trace of a scalar is equal to itself and the cyclic property of trace, we have:

$$\begin{aligned}
MSE_1 &= \text{Tr} (\boldsymbol{\beta}^\top (I - \Sigma X^\top (X \Sigma X^\top + \tau^2 I)^{-1} X)^\top (I - \Sigma X^\top (X \Sigma X^\top + \tau^2 I)^{-1} X) \boldsymbol{\beta}) \\
&= \text{Tr} (\boldsymbol{\beta} \boldsymbol{\beta}^\top (I - \Sigma X^\top (X \Sigma X^\top + \tau^2 I)^{-1} X)^\top (I - \Sigma X^\top (X \Sigma X^\top + \tau^2 I)^{-1} X)) \\
&= \text{Tr} (\boldsymbol{\beta} \boldsymbol{\beta}^\top \Sigma^{-1/2} \Sigma^{1/2} (I - X^\top (X \Sigma X^\top + \tau^2 I)^{-1} X \Sigma) \Sigma^{-1/2} \Sigma \Sigma^{-1/2} (I - \Sigma X^\top (X \Sigma X^\top + \tau^2 I)^{-1} X) \Sigma^{1/2} \Sigma^{-1/2}) \\
&= \text{Tr} (\Sigma^{-1/2} \boldsymbol{\beta} \boldsymbol{\beta}^\top \Sigma^{-1/2} (I - \Sigma^{1/2} X^\top (X \Sigma X^\top + \tau^2 I)^{-1} X \Sigma^{1/2}) \Sigma (I - \Sigma^{1/2} X^\top (X \Sigma X^\top + \tau^2 I)^{-1} X \Sigma^{1/2}))
\end{aligned}$$

Notice $\Pi_\tau = \Sigma^{1/2} X^\top (X \Sigma X^\top + \tau^2 I)^{-1} X \Sigma^{1/2}$ is symmetric. Similarly $I - \Pi_\tau$ is symmetric and so $(I - \Pi_\tau)^2$ is positive semidefinite.

Let $X \Sigma^{1/2} = U D V^\top$ be the singular value decomposition of $X \Sigma^{1/2}$, where $d_1 \leq d_2 \leq \dots \leq d_n$ are the diagonal elements of D (also known as the singular values of $X \Sigma^{1/2}$) arranged in ascending order, then we have:

$$\Pi_\tau = V D^\top U^\top (U D D^\top U^\top + \tau^2 I)^{-1} U D V^\top = V D^\top (D D^\top + \tau^2 I)^{-1} D V^\top$$

which has the same eigenvalues as $D^\top (D D^\top + \tau^2 I)^{-1} D$ by similarity, which are $d_i^2 / (d_i^2 + \tau^2)$ and 0 (repeated $p - n$ times). Likewise the eigenvalues of $I - \Pi_\tau$ are therefore 1 (repeated $p - n$ times) and $\tau^2 / (d_i^2 + \tau^2)$

returning to the bias term, we have:

$$\begin{aligned}
MSE_1 &= \text{Tr} (\Sigma^{-1/2} \boldsymbol{\beta} \boldsymbol{\beta}^\top \Sigma^{-1/2} (I - \Pi_\tau) \Sigma (I - \Pi_\tau)) \\
&\leq \text{Tr} (\Sigma^{-1/2} \boldsymbol{\beta} \boldsymbol{\beta}^\top \Sigma^{-1/2}) \text{Tr} ((I - \Pi_\tau)^2 \Sigma) \\
&\leq \text{Tr} (\Sigma^{-1/2} \boldsymbol{\beta} \boldsymbol{\beta}^\top \Sigma^{-1/2}) \left(\sum_{j=1}^{p-n} \lambda_j + \sum_{j=1}^n \lambda_{p-n+j} \tau^4 / (d_j^2 + \tau^2)^2 \right) \\
&\leq \text{Tr} (\Sigma^{-1/2} \boldsymbol{\beta} \boldsymbol{\beta}^\top \Sigma^{-1/2}) \lambda_1 \left(p - n + \sum_{j=1}^n \tau^4 / (d_j^2 + \tau^2)^2 \right) \tag{35}
\end{aligned}$$

Where we used Von Neumann's trace inequality (Mirsky [1975]) in the penultimate line, on the matrices $(I - \Pi_\tau)^2$ and Σ . So provided τ^2 is small compared to the d_j^2 , MSE_1 decreases approximately linearly in n , as n increases to p .

For the variance term MSE_2 , we once again use the singular value decomposition $X \Sigma^{1/2} = U D V^\top$:

$$\begin{aligned}
 MSE_2 &= \text{Tr}(\mathbb{E}(\boldsymbol{\epsilon}^\top (\Sigma X^\top (X \Sigma X^\top + \tau^2 I)^{-1})^\top \Sigma X^\top (X \Sigma X^\top + \tau^2 I)^{-1} \boldsymbol{\epsilon})) \\
 &= \text{Tr}(\mathbb{E}(\boldsymbol{\epsilon} \boldsymbol{\epsilon}^\top (\Sigma X^\top (X \Sigma X^\top + \tau^2 I)^{-1})^\top \Sigma X^\top (X \Sigma X^\top + \tau^2 I)^{-1})) \\
 &= \tau^2 \text{Tr}((X \Sigma X^\top + \tau^2 I)^{-2} X \Sigma^2 X^\top) \\
 &= \tau^2 \text{Tr}((U D D^\top U^\top + \tau^2 I)^{-2} U D V^\top \Sigma V D^\top U^\top) \\
 &= \tau^2 \text{Tr}(U^\top (U D D^\top U^\top + \tau^2 I)^{-1} U U^\top (U D D^\top U^\top + \tau^2 I)^{-1} U D V^\top \Sigma V D^\top) \\
 &= \tau^2 \text{Tr}(V D^\top (D D^\top + \tau^2 I)^{-2} D V^\top \Sigma) \\
 &\leq \tau^2 \sum_{j=1}^n \lambda_1 d_j^2 / (d_j^2 + \tau^2)^2
 \end{aligned}$$

Where the last line again follows from Von Neumann's trace inequality, on the matrices $V D^\top (D D^\top + \tau^2 I)^{-2} D V^\top$ and Σ . ■